

Sodium-Oxygen Batteries: A Comparative Review from Chemical and Electrochemical Fundamentals to Future Perspective

Hossein Yadegari, Qian Sun, and Xueliang Sun*

Alkali metal-oxygen (Li-O₂, Na-O₂) batteries have attracted a great deal of attention recently due to their high theoretical energy densities, comparable to gasoline, making them attractive candidates for application in electrical vehicles. However, the limited cycling life and low energy efficiency (high charging overpotential) of these cells hinder their commercialization. The Li-O₂ battery system has been extensively studied in this regard during the past decade. Compared to the numerous reports of Li-O₂ batteries, the research on Na-O₂ batteries is still in its infancy. Although, Na-O₂ batteries show a number of attractive properties such as low charging overpotential and high round-trip energy efficiency, their cycling life is currently limited to a few tens of cycles. Therefore, understanding the chemistry behind Na-O₂ cells is critical towards enhancing their performance and advancing their development. Chemical and electrochemical reactions of Na-O₂ batteries are reviewed and compared with those of Li-O₂ batteries in the present review, as well as recent works on the chemical composition and morphology of the discharge products in these batteries. Furthermore, the determining kinetics factors for controlling the chemical composition of the discharge products in Na-O₂ cells are discussed and the potential research directions toward improving Na-O₂ cells are proposed.

1. Introduction

Lithium-ion (Li-ion) batteries have been considered as a state of the art technology for energy storage applications ranging from use in portable electronic devices all the way to electrical vehicles (EVs).^[1] However, Li-ion battery systems cannot adequately meet the growing demand required for energy storage in extended range EVs.^[2] Metal-O₂ batteries on the other hand are among the limited number of battery systems that can appropriately compete with gasoline in terms of theoretical energy density. As a result, metal-O₂ batteries are considered as the next generation energy storage system with potential applications in electrical transportation. The high energy density of metal-O₂ cells is a product of coupling a high energy metal as the negative electrode with an air electrode that utilizes oxygen

as the positive electrode material. Among the various metal-O₂ systems, Li- and Na-O₂ (alkali metal-O₂) batteries exhibit the highest theoretical specific energies of 11430 and 3451 Wh/kg, respectively (based on only the weight of negative electrode materials).^[3,4] The accumulation of oxygen during the discharge reaction considerably increases the weight of electrode material. Considering the weight of positive electrode material in the theoretical energy density calculation of alkali metal-O₂ cells gives a more realistic value of 3505 and 1602 (1105) Wh/kg for Li- and Na-O₂ cells (based on the discharge products of Li₂O₂ and Na₂O₂ (NaO₂)), respectively.

Studies on Na-O₂ batteries was triggered by Peled et al. who reported a battery system working at temperatures above the melting point of sodium metal (98 °C) as an alternative battery system to Li-O₂.^[5] Their initial work was followed by Sun et al. who introduced the first rechargeable Na-O₂ cell at room temperature.^[6] However, further development of alkali metal-

O₂ cells is generally restricted by their poor cycling capability and high charging overpotential which results in decreased energy efficiency. In addition, major components of the cells such as the electrolyte and carbonaceous air electrode have been shown to undergo chemical and electrochemical decomposition reactions, especially at higher potentials.^[7–14] Chemical composition of the discharge products is among the major contributing factors that results in a high charging overpotential. Although lithium peroxide (Li₂O₂) is well accepted to be the major discharge product of Li-O₂ in the presence of stable electrolytes, the chemical composition of Na-O₂ cell product is still a point of controversy. Both sodium peroxide (Na₂O₂) and superoxide (NaO₂) are almost evenly identified as the major discharge product.

Liu et al. and Li et al. reported the formation of Na₂O₂ in Na-O₂ cell using an ether-based electrolyte with a charging overpotential of ≈1.5 V.^[15,16] A hydrated form of sodium peroxide (Na₂O₂·2H₂O) has also been found in other studies.^[17,18] Hartmann et al. found unique micrometer structures of cubic NaO₂ as the major discharge product of Na-O₂ cells which were decomposed below 2.5 V vs Na/Na⁺ (charging overpotential of ≈0.2 V).^[4,19,20] Furthermore, using differential electrochemical mass spectrometry (DEMS) analysis, McCloskey et al.

Dr. H. Yadegari, Q. Sun, X. Sun
Department of Mechanical and Materials Engineering
University of Western Ontario
London, Ontario N6A 5B9, Canada
E-mail: xsun@eng.uwo.ca



DOI: 10.1002/adma.201504373

showed that the discharge product of a Na-O₂ cell is predominantly NaO₂.^[21] More recently, Zhao et al. disclosed that NaO₂ is the main product under static oxygen atmosphere, while Na₂O₂·2H₂O was obtained under flowing oxygen gas.^[22] A combination of NaO₂ and Na₂O₂ and/or Na₂CO₃ is also reported in other studies.^[23–26] A summary of the reported discharge products for Na-O₂ battery system is presented in **Table 1**. Theoretical calculations have also been applied to predict the discharge product of Na-O₂ cell. NaO₂ has been suggested by first-principle DFT calculations to be stable discharge product of Na-O₂ cells under the standard conditions (300 K and 1 atm).^[27] In an interesting study conducted by Cedar et al., calculation on the surface energies of various sodium oxide crystals with energy of bulk compounds, demonstrated that bulk Na₂O₂ is a more stable phase under standard operating conditions and NaO₂ is more stable at the nanoscale and/or under elevated oxygen partial pressures.^[28]

Although Na-O₂ batteries have demonstrated lower charging overpotentials compared to Li-O₂, the cycling life of the cell is still limited to a few tens of cycles. The poor cycling life of Na-O₂ cell is a result of multiple challenges associated with the main components of the cell, i.e., negative and positive electrodes and electrolyte. The major challenges facing Na-O₂ cells are summarized in **Figure 1**. Some of these challenges are in common with Li-O₂ cells and are related to the negative electrode and electrolyte. Dendrite formation on the negative sodium metal electrode during consecutive dissolution and deposition of sodium is even more severe than that found for lithium metal electrodes.^[19,22] Formation of the dendrite structure results in destruction of the sodium metal electrode via corrosion/passivation as well as consumption of the cell electrolyte due to continuous SEI formation on high surface area dendritic structures. In addition, sodium metal exhibits greater sensitivity toward trace amounts of moisture and dissolved oxygen into the cell electrolyte compared to metallic lithium. Therefore, sodium protection is a major challenge that should be addressed to enhance the cycling life of the Na-O₂ cells. In addition, instability of available organic electrolytes against oxidation and decomposition by superoxide intermediates and/or discharge products of the cell is another major challenge facing both Li- and Na-O₂ cells.^[29] Decomposition of the organic electrolyte within cells results in the production of insulating carbonate-based parasitic products which ultimately contributes in raising the charging overpotential of the cell. Higher charging potential also results in increased electrolyte decomposition.^[8,12,30] Finding an appropriate electrolyte with adequate chemical stability and wide electrochemical window will greatly improve the cyclability of both cells. Furthermore, instability of the polymeric binders and electrolyte salts in the highly oxidative environment of the alkali metal-O₂ cells are among other challenges that need to be addressed.

In addition to the common challenges facing Li- and Na-O₂ cells, there are contradictory findings over the chemical composition of discharge products produced in Na-O₂ cell. While the cells with NaO₂ discharge product exhibit a very low charging potential, the overpotential in the case of cells with Na₂O₂ as the product is comparable with that of Li-O₂. Since lower charging overpotential of Na-O₂ cells is a principle advantage over Li-O₂, controlling the composition of the discharge product will play a



Hossein Yadegari is currently a Ph.D. candidate at the University of Western Ontario (UWO), Canada. He received his B.Sc. (applied chemistry) from Sharif University of Technology (Tehran, Iran) in 2005 and M.Sc. and Ph.D. (analytical chemistry) from K. N. Toosi University of Technology (Tehran, Iran) in 2012. Then he joined

Prof. Xueliang (Andy) Sun's Nanomaterials and Energy Group at UWO to conduct his second Ph.D. on materials science and engineering. His main research interests are associated with energy conversion and storage, electrochemistry of nanomaterials and electrocatalysis. His current research is focused on developing nanostructured air electrodes for alkali metal-oxygen cells.



Qian Sun is a postdoctoral fellow in Prof. Xueliang (Andy) Sun's Group at the University of Western Ontario, Canada. He received his B.S. degree in Chemistry in 2006, M.S. degree in Physical Chemistry in 2009, and Ph.D. degree in Applied Chemistry in 2013 at Fudan University, China, under the supervision of Prof. Dr. Zheng-Wen Fu on

the study of Li-/Na-ion batteries and Na-air batteries. He joined Prof. Sun's group in 2013 and his current research interests focus on Na-air, Na-S, and Na-ion batteries as well as solid-state Li/Na batteries.



Xueliang (Andy) Sun is a Senior Canada Research Chair (Tier 1) and a Full Professor at the University of Western Ontario, Canada. He received his Ph.D. in Materials Chemistry under the direction of Prof. George Thompson in 1999 at the University of Manchester, UK, followed by work as a postdoctoral fellow under the direction of

Prof. Keith Mitchell at the University of British Columbia, Canada and as a Research Associate under the direction of Prof. Jean-Pol Dodelet at l'Institut National de la Recherche Scientifique (INRS), Canada. His current research interests are associated with synthesis of advanced nanomaterials for electrochemical energy storage and conversion including PEM fuel cells, lithium ion batteries and metal-air batteries.

Table 1. A summary of the reported discharge products for Na-O₂ battery system.

Electrolyte	Discharge product	Charge potential	Ref.
0.5 M NaSO ₃ CF ₃ in PC	Na ₂ CO ₃	3.5–4.25 V	[25]
1 M NaClO ₄ in PC	Na ₂ CO ₃	> 4 V	[17]
1 M NaPF ₆ in 1:1 EC/DMC	Na ₂ O ₂ + Na ₂ CO ₃	3.5–4 V	[6]
1 M NaClO ₄ in DME	Na ₂ O ₂ + Na ₂ CO ₃	3–4 V	[83]
1 M NaClO ₄ in PC	Na ₂ O ₂ + Na ₂ CO ₃	3–4 V	[24]
0.5 M NaSO ₃ CF ₃ in DEGDME	Na ₂ O ₂	3–3.5 V	[16]
0.25 M NaPF ₆ in DME	Na ₂ O ₂	~4 V	[15]
0.1 M NaClO ₄ (+ 0.001 M NaI) in DME	Na ₂ O ₂	2.3–3.2 V	[126]
1 M NaClO ₄ in TEGDME	Na ₂ O ₂ ·2H ₂ O	2.5–4 V	[17]
0.5 M NaSO ₃ CF ₃ in DEGDME	Na ₂ O ₂ ·2H ₂ O	2.5–4 V	[18]
0.5 M NaSO ₃ CF ₃ in DEGDME	Na ₂ O ₂ ·2H ₂ O + NaO ₂	2.3–4 V	[26]
0.5 M NaSO ₃ CF ₃ in TEGDME	Na ₂ O ₂ ·2H ₂ O/NaO ₂	2.5–3.5 V	[22]
1 M NaSO ₃ CF ₃ in TEGDME	Na ₂ O ₂ + NaO ₂	2.5–4 V	[23]
0.5 M NaSO ₃ CF ₃ in DEGDME	Na ₂ O ₂ + NaO ₂	2.4–4.5 V	[84]
0.5 M NaSO ₃ CF ₃ in DEGDME	Na ₂ O ₂ + NaO ₂	2.3–4.2 V	[30]
0.5 M NaSO ₃ CF ₃ in DEGDME	NaO ₂	~2.3 V	[4, 19, 40]
0.2 N NaSO ₃ CF ₃ in DME	NaO ₂	~2.5 V	[21]
0.1 M NaClO ₄ in DME	NaO ₂	~2.3 V	[31]
0.1 M NaSO ₃ CF ₃ in DEGDME	NaO ₂	2.5 V	[105]

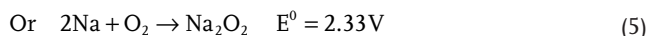
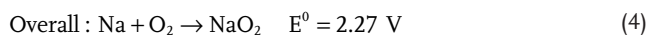
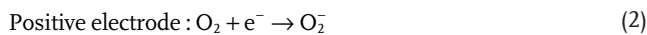
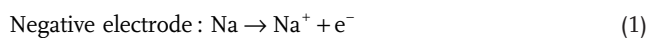
vital role here. Moreover, chemical instability of produced NaO₂ discharge products is also reported by some researchers.^[31] Therefore, a deep understanding pertaining to the composition and stability of the discharge products in Na-O₂ cell is critical for further improvement. Here, the effect of various physico-chemical parameters on the composition and morphology of the discharge product of non-aqueous Na-O₂ cells is discussed. The chemical and electrochemical reaction mechanisms of the cell from various perspectives including kinetic parameters, humidity effect, air electrode, binders, electrolyte, and catalysts are summarized and discussed in detail. Furthermore, several potential research directions toward enhanced alkali metal-O₂ batteries based on the comparison of Na-O₂ with Li-O₂ battery systems are proposed. We try to clarify the behavior of Na-O₂ cell from chemical and electrochemical points of view.

2. Principles of Na-O₂ cell

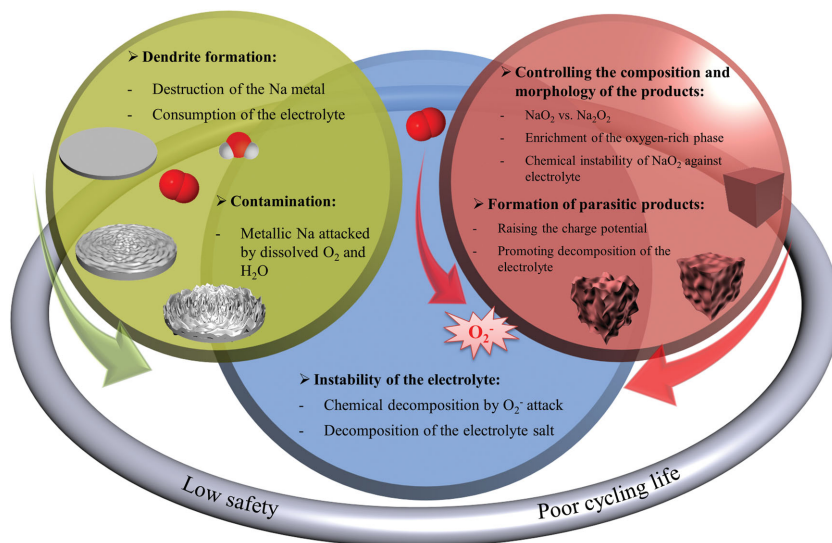
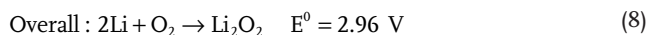
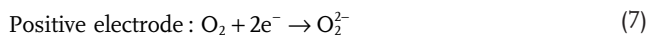
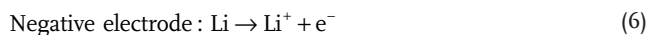
2.1. Electrochemical Reactions in Na-O₂ Cell

Metal-O₂ cells employ a dissolution/precipitation reaction during the electrochemical process rather than intercalation mechanism. In contrast to the intercalation reaction, a dissolution/precipitation reaction involves

an evolution in the crystal structure of the electrode material. The working mechanism of Na-O₂ cells is schematically illustrated in **Figure 2**. Briefly, Na metal is oxidized to form Na⁺ ions during the discharge cycle of the cell. Na⁺ ions then move through the electrolyte toward the cathode electrode, where oxygen molecules become reduced and combine with Na⁺ ions to form sodium oxide discharge products. Following cell discharge, the metal anode will be thoroughly converted to metal oxides which are insoluble in the aprotic electrolyte of the cell and accumulate on the surface of the air electrode. In order to accommodate the extra discharge product, the air electrode must possess appropriate porosity with large void volume. The electrochemical reactions occurring during the discharge cycle of the Na-O₂ cell can be represented in the following chemical equations:



Similar electrochemical reactions take place in the case of Li-O₂ cell:

**Figure 1.** Major challenges of Na-O₂ cell.

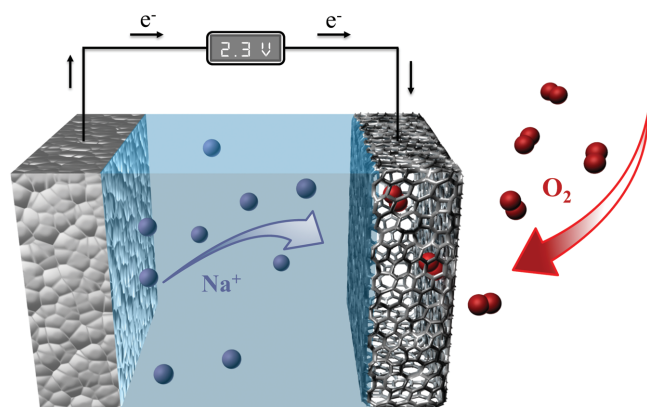
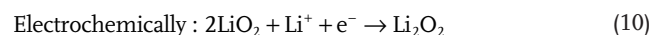
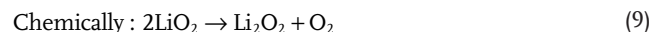


Figure 2. Schematic diagram of Na-O₂ cell.

According to Bruce et al.,^[7,8] the oxygen reduction reaction (ORR) in non-aqueous electrolytes involves the formation of a superoxide (O₂⁻) intermediate. The odd number of electrons makes the superoxide ion extremely unstable resulting in rapid reaction with surrounding Li⁺ ions to produce lithium superoxide (LiO₂). However, the small Li⁺ ion is not capable of stabilizing the extremely unstable O₂⁻. As a result, LiO₂ disproportionates to lithium peroxide (Li₂O₂) either chemically or electrochemically via following reaction routes:



Using an interesting electrochemical approach, Abraham et al.^[32] demonstrated that the superoxide intermediate can be stabilized in a non-aqueous solution containing tetrabutylammonium (TBA) cation. Cyclic voltammetry (CV) test for oxygen reduction and evolution (OER) reactions in acetonitrile solution containing TBA⁺ ion with two different counter ions exhibited two pairs of redox peaks (Figure 3a): a reversible and a quasi-reversible pair with peak potential separations of ~ 0.6 and ~ 2 V (vs Ag/AgCl), respectively. The peak potential separation of ~ 0.6 V, in the case of reversible pair (denoted as E_{p1} and E_{p3} in Figure 3a), is characteristic of a one electron transfer reaction ($\Delta E_p = 0.592/nV$ where n = number of transferred electrons)^[33] and has been related to the O₂/O₂⁻ redox coupling reaction. The E_{p1} reduction peak is also followed by a second reduction peak which has been correlated to the reduction of O₂⁻ to O₂²⁻. Oxidation of O₂²⁻ does not typically occur until applying a large overpotential of over 2 V. So, the quasi-reversible redox pair of E_{p2}/E_{p4} can be correlated to the O₂/O₂²⁻ redox couple. However, oxygen exhibits different electrochemical behavior in the presence of other alkali metal ions (Figure 3b). Only one oxygen reduction peak, corresponding to the O₂/O₂⁻ redox couple, can be seen during the cathodic potential sweep of LiPF₆ electrolyte salt under a scan rate of 100 mV s⁻¹, demonstrating the rapid deterioration of O₂⁻ in the presence of Li⁺ via a chemical reaction. In the case of Na⁺ cation, a shoulder-like peak related to the reduction of O₂⁻ to O₂²⁻ also appears in the voltammogram, corresponding to the elevated chemical stability of O₂⁻ in the presence of Na⁺. Equivalent oxidation

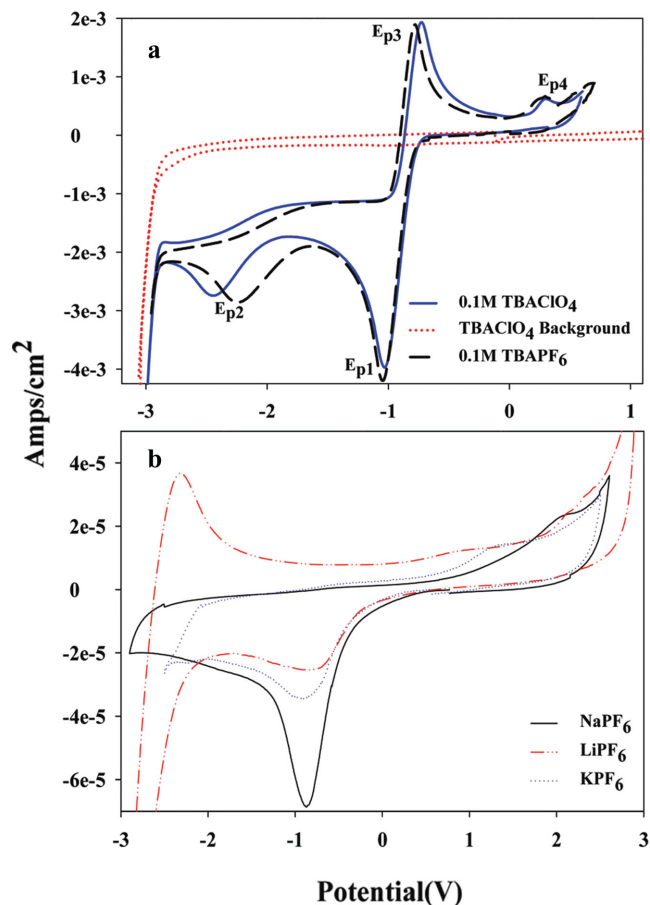


Figure 3. a) Cyclic voltammograms of a glassy carbon electrode (vs Ag/AgCl) for the reduction of oxygen in the presence of 0.1 M TBAPF₆ (black), 0.1 M TBAClO₄ (blue), and the argon background (dotted) in MeCN solution. b) Cyclic voltammograms of a glassy carbon electrode (vs Ag/AgCl) for the oxygen reduction in the presence of 0.1 M LiPF₆ (dashed line), 0.1 M NaPF₆ (solid line), and KPF₆ (dash-dotted line) in MeCN solution. (Scan rate = 100 mV s⁻¹). Reproduced with permission.^[32] Copyright 2009, American Chemical Society.

evolution peaks also appear after applying overpotentials of more than 2 V for both of lithium and sodium. The reduction peak of O₂⁻ to O₂²⁻ is truly well-defined and distinguishable in the presence of K⁺ cation and two oxygen evolution peaks can also be identified during the anodic sweep. A similar comparison for oxygen electrochemical behavior in presence of TBA⁺, K⁺ and Li⁺ cations are presented elsewhere.^[34]

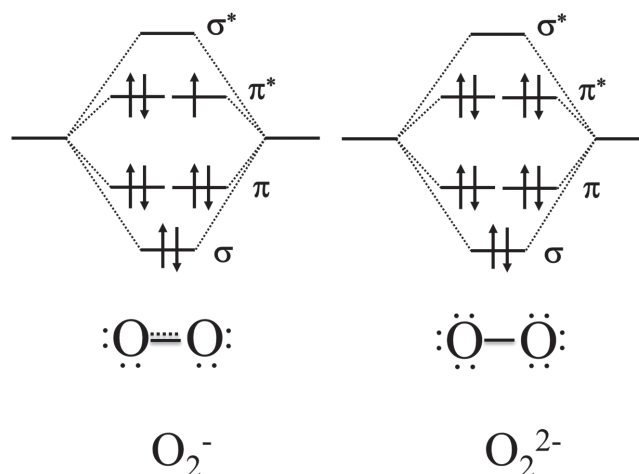
Abraham's electrochemical study on the ORR and OER in non-aqueous electrolyte illustrates how the stability of the superoxide ion can be altered through the presence of cations with relatively larger radii. The increased stability of superoxide ion coupled with a large cation has been explained using hard and soft acid and base (HSAB) theory.^[32,35] Larger cations, which are considered as soft Lewis acid, exhibit higher polarizability and can more effectively stabilize the superoxide ion, which is a soft Lewis base. In other words, the stability of the electrochemically produced alkali metal superoxide increases from lithium to potassium (KO₂ > NaO₂ > LiO₂). While LiO₂ is thermodynamically unstable at standard conditions, KO₂ is a

stable and commercially available product. These findings are also in good accordance with the detected discharge products of alkali metal- O_2 cells: the discharge product of Li- O_2 cell (in a relatively stable electrolyte and on a stable air electrode) is well-known to be Li_2O_2 .^[36–38] Both NaO_2 and Na_2O_2 are reported to be formed as the discharge products of Na- O_2 cell under different physicochemical conditions;^[4,15,17,18,21–23,39,40] and KO_2 is proved to be the major discharge product of K- O_2 cells.^[34] The chemistry of discharge products in Li- and Na- O_2 cells will be discussed in more details in the next sections.

2.2. Chemistry of Sodium and Sodium Oxides

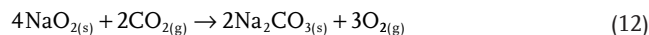
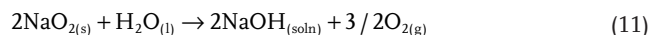
Sodium (Na, atomic number = 11), is a highly reactive alkali metal and is the seventh most abundant element and fifth most abundant metal in the earth's crust. The ease of sodium metal production (via electrolysis of fused sodium salts) makes it extremely inexpensive, especially compared to lithium. Another advantage of sodium over lithium for application as the anode electrode material for metal-air batteries is its stability against the formation of nitride which is important for development of Na-“air” batteries. Sodium is the second most electropositive metal after lithium ($M^+_{(aq)} + e^- \rightarrow M_{(s)}$; $E^0 = -3.045$ and -2.714 V for $M = Li$ and Na , respectively) which makes it a desirable candidate as an anode material.^[41] However, the increased atomic weight of sodium ($22.989 \text{ g mol}^{-1}$) over lithium (6.941 g mol^{-1}) dramatically decreases the theoretical specific capacity of the anode electrode material from 3861 mAh g^{-1} for lithium to 1166 mAh g^{-1} for sodium. These specific capacities correspond to a theoretical energy density value of 11757 and 3164 Wh kg^{-1} for lithium and sodium, respectively.

The relatively low first ionization energy of alkali metals (ns^1) is responsible for the high chemical reactivity and common +1 oxidation state of these elements. Alkali metals form a variety of binary compounds with oxygen including M_7O , M_4O , M_3O , M_2O suboxides, M_2O normal oxides, M_2O_2 peroxides, M_2O_3 sesquioxides, MO_2 superoxides (also referred to as hyperoxide) and MO_3 ozonides.^[42] The stability of the oxygen-rich compounds increases with atomic number and both of lithium and sodium form stable oxide and peroxide phases. Interestingly, the sodium superoxide phase is stable at standard ambient temperature and pressure ($25 \text{ }^\circ\text{C}$ and 1atm , referred to as SATP), but lithium cannot form a stable superoxide phase above 15 K . Sodium superoxide (NaO_2) can be considered as an ionic molecular crystal which is composed of sodium and paramagnetic superoxide (O_2^-) ions. O_2^- ion has nine electrons at the $2p$ molecular levels with the electronic configuration of $\sigma_g^2 \pi_u^4 \pi_g^3$ (Scheme 1). The remained unpaired electron is responsible for the paramagnetic properties of the superoxide phase.^[43,44] This electron configuration also increases the covalent bond order between the two oxygen atoms to 1.5 (compared with bond order of 1 in O_2^{2-}). As a result, the O-O interatomic distance decreases from 1.60 in O_2^{2-} to 1.35 \AA in O_2^- .^[45] O_2^- ion is not active in the infrared region, but has a dipole-allowed $\pi_u \rightarrow \pi_g$ transition in the visible region which is responsible for the yellow to orange color typically seen for superoxide compounds.^[46] Furthermore, O_2^- is a strong oxidizing agent which can facilitate the oxidation of organic materials to carbonate

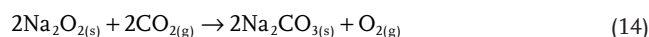
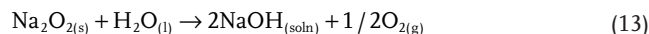


Scheme 1. The electronic structure of peroxide and superoxide ions.

species and also reacts with water and carbon dioxide in the following manner:^[42,47]



Sodium peroxide on the other hand is an ionic molecular compound which is composed of sodium and peroxide (O_2^{2-}) ions. O_2^{2-} contains a single covalent bond with an electronic configuration that is isoelectronic with F_2 (see also Scheme 1). Na_2O_2 is stable toward the thermal decomposition reaction in the absence of oxygen or other oxidizable compounds up to $675 \text{ }^\circ\text{C}$. O_2^{2-} ion does not show any absorption in the visible region and appear colorless in its compounds, however, the peroxides of the heavier alkali metals are colored. Na_2O_2 appears pale yellow in color due to the contamination by superoxide.^[47,48] Na_2O_2 is extremely hygroscopic and tends to form peroxide hydrates in the presence of water or water vapor. Peroxide hydrates are also less thermally stable and more reactive toward reactions with carbon dioxide compared to their anhydrous counterparts. Na_2O_2 is also a strong oxidizing agent and reacts with water and carbon dioxide in the following reaction mechanism:^[42,47]



2.3. Components of the Na- O_2 Cell

2.3.1. Cathode

Na- O_2 cells employ oxygen as the positive electrode material which is being reduced and combines with Na^+ ion to form solid sodium oxide during the discharge cycle of the cell. The air electrode in Na- O_2 cells provides a three-phase zone, where

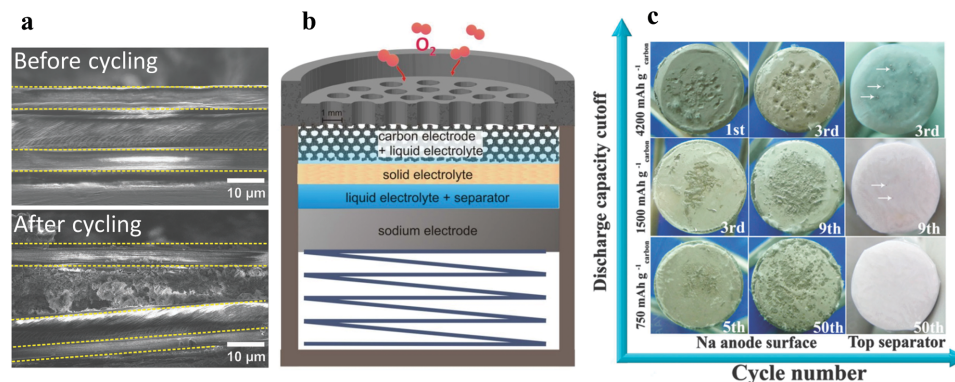


Figure 4. a) Cross section SEM images of a pristine separator and one after cycling. b) Application of a Na-beta-alumina solid electrolyte membrane (0.5 mm thickness) as barrier for dendrite growth. a-b) Reproduced with permission.^[19] Copyright 2013, Royal Society of Chemistry. c) Optical images of the Na anode surfaces and separators under different cycling conditions. The surface roughness increases upon increasing the cutoff discharge capacity as well as the cycle number due to the Na dendrit growth. c) Reproduced with permission.^[22] Copyright 2014, Royal Society of Chemistry.

oxygen reduction and evolution reactions occur. Furthermore, the air electrode also serves as a medium to accommodate the solid discharge product produced during the electrochemical process. The air electrode in Na-O₂ cells plays a similar role to the one found in Li-O₂ cells, a comprehensive discussion of this can be found in references.^[49–52] Briefly, an ideal air electrode should have adequate porosity along with appropriate pore volume and pore sizes distribution, in addition to the general characteristics of electrodes materials such as electronic conductivity, chemical stability, high surface area and low cost. The porous structure is responsible for oxygen diffusion as well as allowing for the formation and storage of discharge products and also decomposition of the produced discharge products during the charge cycle. In addition, the final performance of the metal-air systems strongly depends on the efficiency of the air electrode. Many publications have demonstrated that the discharge capacity of the metal-O₂ cells is often limited by the air electrodes capacity to adequately store discharge product. The ability of the air electrode to accommodate the discharge products determines the discharge capacity of the electrode and hence the whole battery.^[53]

2.3.2. Anode

Despite the extremely high energy density of lithium metal as an anode material, the formation of Li dendrites during repeated charge/discharge processes severely limits its capabilities.^[52] Similar issue restricts the cyclability of sodium metal negative electrodes in Na-O₂ cells.^[19,22] Dendrite formation is a result of sequential accumulation and cracking of a solid electrolyte interface (SEI) layer in the presence of incompatible organic electrolytes. Dendritic structures may ultimately penetrate into the separator; reach the positive electrode and create a short circuit within the battery, resulting in smoke or even fire, especially in presence of volatile organic electrolytes. The anode material is also destroyed from corrosion and passivation of the dendrite structures during battery cycling. In addition, continuous formation of SEI layer on high surface area dendritic structures results in consumption of the electrolyte, compromising the cycle life of the battery.^[52]

Hartmann et al. observed the growth of sodium dendritic structures penetrating into the pores of the polymer separator material during the cycling of Na-O₂ cells (Figure 4a).^[19] Energy dispersive spectroscopy (EDS) analysis revealed that the dendritic structure is composed of both sodium and oxygen. The authors also suggested that the dendrite formation in Na-O₂ cell may be physically suppressed by separating the anode and the cathode using a solid ion conducting membrane such as sodium-beta-alumina (Figure 4b). The formation of sodium dendritic structures is also reported by Zhao et al.^[22] The authors visually investigated the sodium anode electrode during the Na-O₂ cell cycling under various discharge capacity cut-off values (Figure 4c). It was observed that the surface of the sodium anode electrode becomes rougher with increasing discharge capacity and cycle number. Two approaches may be followed as the potential solutions for suppressing anode dendrite formation. The first involves mechanical suppression of the dendritic structure by using an interfacial or protective layer (also called ex situ or artificial SEI) comprised of Na-ion conductive polymers, ceramics or glass on the anode electrode. The softer nature of sodium metal compared to lithium might be specifically beneficial in this regard. The second approach involves the in situ formation of a stable SEI layer using various organic solvents, sodium salts and/or functional additives. Contamination of the metal negative electrode by moisture and oxygen from the positive electrode is another difficulty associated with the utilization of sodium metal in Na-O₂ cells. Replacing of sodium metal with a sodiated carbon electrode may address this issue in cost of compromising on the energy density of the cell.^[54] An appropriate protective layer, however, would undoubtedly improve the cyclability and safety of sodium metal negative electrodes for application in Na-O₂ batteries.

2.3.3. Electrolyte

Stability of the electrolyte is a severe challenge currently facing the development of alkali metal-O₂ batteries, even at the research scale. An ideal electrolyte should tolerate the highly oxidative environment of the cells for a long cycling life and facilitate the reversible formation and decomposition of the

discharge product. It is well-recognized that the electrolyte not only affects the oxygen reduction and evolution reaction mechanisms, but also the chemical composition of the discharge products as well as the reversibility of the cell.^[29] Carbonates are common solvents for non-aqueous batteries due to their high stability and low volatility. Therefore, similar to the Li-O₂ battery system, early research conducted on Na-O₂ was done using carbonate based electrolytes. In these studies sodium carbonate was reported as the major discharge products.^[6,17] However, later studies revealed that carbonate based solvents are unstable against the nucleophilic attack by the superoxide (O₂⁻) intermediate in Li-O₂ environment.^[55,56] In addition, the superoxide anion radical reacts with the etheral carbon atom of organic carbonates, resulting in a ring opening mechanism and the formation of peroxy anion (ROO⁻) species, which is even more reactive than the preliminary superoxide. Accordingly, carbonate-based electrolytes decompose to form high molecular weight products including carbonates and alkyl carbonates.^[29]

Afterward, ether-based electrolytes, which are believed to be more stable than carbonates, were employed in most of the studies on Na-O₂ cells. Ethers are more stable than carbonates toward nucleophilic attacks by superoxide intermediates and have relatively low vapor pressure. Furthermore, ether based electrolytes display an extended oxidation potential window up to 4.5 V versus Li/Li⁺ and hence might be considered as good candidates for Na-O₂ cells. Nevertheless, recent studies on Li-O₂ battery system revealed that Li₂O₂ produced during the first discharge of the cell using an ether-based electrolyte also contains electrolyte decomposition products, resulting in a mixture of lithium carbonate, lithium alkyl carbonates, polyethers/esters, CO₂, and H₂O.^[13] Therefore, studies toward finding a truly stable electrolyte for both Na- and Li-O₂ battery systems is an ongoing research subject. Besides, the hybrid electrolyte system based on two different electrolytes in the same cell, i.e., an aqueous electrolyte on the cathode side (catholyte) and an aprotic electrolyte on the anode side (anolyte) is also examined for Na-O₂ cell by number of researchers.^[57–60]

3. Charging Overpotential in Na-O₂ Cells

3.1. Theoretical Calculations

As discussed above, the charging overpotential of Na-O₂ cell is greatly dependent on the chemical composition of the discharge product. Theoretical calculations have been employed to estimate the discharge products of Na-O₂ cell. In a comparative study, Lee et al.^[27] used first-principle calculations to develop a

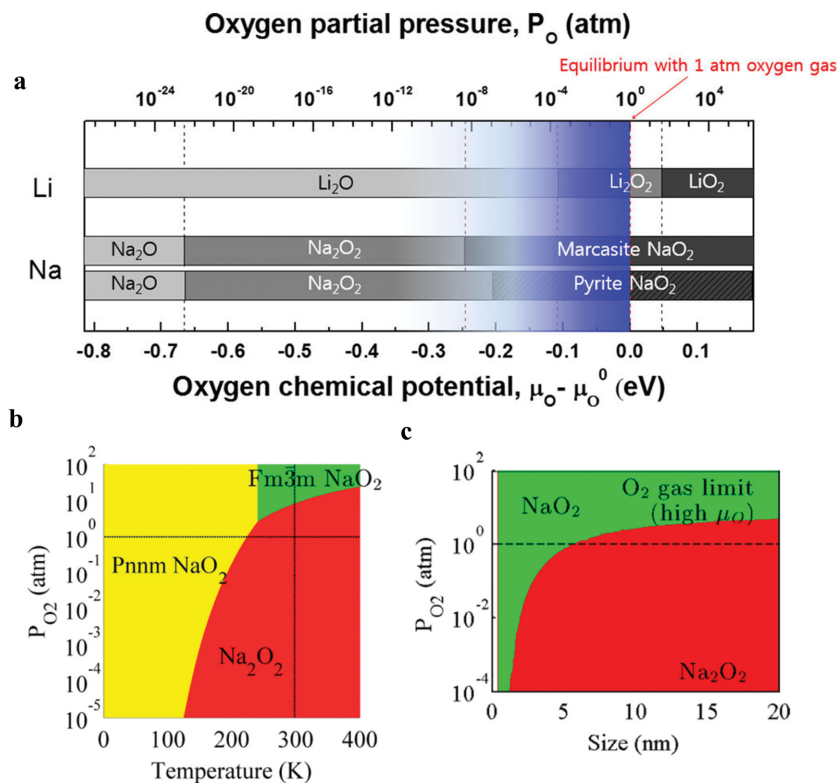


Figure 5. a) Phase stability map of various lithium/sodium oxides as a function of oxygen chemical potential or oxygen partial pressure. The blue region shows the oxygen chemical potential range under nonequilibrium conditions that can result from fast consumption of O₂ in the electrolyte during discharge. a) Reproduced with permission.^[27] Copyright 2014, American Chemical Society. b) Phase diagram of Na-O as function of temperature and O₂ partial pressure. c) Phase diagram of Na₂O₂ (red) and NaO₂ (green) at 300 K as a function of particle size and P_{O₂} at the O₂ gas limit. b-c) Reproduced with permission.^[28] Copyright 2014, American Chemical Society.

phase stability map of discharge products for Li- and Na-O₂ cells as a function of oxygen partial pressure. It was concluded that under standard experimental conditions of T = 298 K and P_{O₂} = 1 atm, Li₂O₂ and NaO₂ are the stable discharge products for Li- and Na-O₂ cells, respectively (Figure 5a). According to the authors, NaO₂ is the discharge product of the Na-O₂ cells even under the reduced oxygen partial pressure down to 10⁻⁸ atm. Na₂O₂ and Na₂O are proposed as the most stable phases under lower oxygen pressures. However, for Li-O₂ cells, Li₂O₂ was found to be the most stable phase under standard experimental conditions and Li₂O is predicted to be the product of the cell under lower oxygen partial pressure. LiO₂ is argued to be energetically stable only under oxygen partial pressures higher than 40 atm. The larger ionic radius of Na compared to Li is thought to contribute in the stabilization of the superoxide ion.

These results are in contrast with the finding of Ceder's research group^[28] who predicted that Na₂O₂ is the stable bulk phase for sodium oxide under standard experimental conditions. In the latter study, Ceder et al. used first principle calculations to investigate the thermodynamic stability of various sodium oxides as a function of temperature, oxygen partial pressure and particle size of the discharge product. The formation free energies of sodium oxides were calculated as a function of temperature and oxygen partial pressure by combining

the phonon energy of solids with the chemical potential of oxygen at various pressures and temperatures. The results have been used to plot the equilibrium T/P_{O_2} phase diagram for Na-O system (Figure 5b). Na_2O_2 is proposed to be the stable phase under standard condition and also under higher temperatures or lower oxygen pressures. Based on the equilibrium T/P_{O_2} phase diagram, NaO_2 is only thermodynamically stable at oxygen partial pressures higher than 8.5 atm (room temperature). By entering the surface energies of the polymorphs for two competing sodium oxides into the calculations, the authors were able to calculate the phase diagram as a function of particle size and oxygen partial pressure for Na_2O_2 and NaO_2 (Figure 5c). It was concluded that the formation of NaO_2 is preferred when the particle size of the product decreases to nanometer scale, since the surface energies of NaO_2 are lower than those of Na_2O_2 . The crossing point at the standard oxygen partial pressure of 1 atm points to a threshold particle size of around 6 nm for NaO_2 product. In addition, NaO_2 exhibited a lower critical nucleation energy barrier compared to Na_2O_2 suggesting that NaO_2 particles are more likely to nucleate. Similar to aforementioned theoretical calculations, contradictory results over stability of NaO_2 and Na_2O_2 were also obtained in experimental studies which are discussed in the following section.

In order to determine the reason behind the lower charging overpotential for NaO_2 compared to Na_2O_2 , Siegel's research group used density functional and quasi-particle GW methods to calculate the theoretical conductivity values for these species.^[61] The calculated ionic and electronic conductivity values for NaO_2 and Na_2O_2 are listed and compared with those of Li_2O_2 in Table 2. The group determined that the charge transport is limited by sluggish charge hopping between O_2 dimers in all cases. The calculated conductivity values suggest that both NaO_2 and Na_2O_2 possess rather large band gaps that are greater than 5 eV, suggesting that both these species are electrically insulating. The calculated band gap for Na_2O_2 is in reasonable agreement with the value of 4.84 eV calculated by Araujo et al.^[62] While a hole polaron migration is thought to be the main route for charge diffusion in Na_2O_2 ,^[62] a combination of electron and hole polarons are proposed to be responsible for charge transport in NaO_2 . The authors concluded that the lower charging overpotential for NaO_2 cannot be explained by the enhanced electrical conductivity of NaO_2 over Na_2O_2 . On the other hand, the ionic conductivity of NaO_2 was predicted to be 10 orders of magnitude higher than Na_2O_2 , mainly originating from p-type conduction stemming from positive oxygen dimer vacancies as well as n-type conduction from negative sodium vacancies. However, the authors discommend the contribution of ionic conductivity toward the lower charging overpotential of NaO_2 ,^[63] instead the authors suggest that decomposition of the

electrolyte is the major contributing factor for a lower charging overpotential.

These results are in good accordance with a DFT study conducted by Arcelus et al. on the electronic structure of NaO_2 .^[64] The authors studied the effect of atomic structure and morphology on the electronic properties of NaO_2 phase. Various model systems including bulk NaO_2 , extended (100) surface, and small $(NaO_2)_n$ clusters were investigated in this study using the Perdew-Burke-Ernzerhof (PBE) gradient-corrected functional and the Heyd-Scuseria-Ernzerhof (HSE06) hybrid density functional. The results indicate the formation of a fully occupied spin-up and half-filled spin-down antibonding states in the valence band for all systems. The empty O 2p states were calculated using hybrid HSE06 functional to appear above the Fermi level with band gaps larger than 2 eV, revealing the insulating nature of all investigated systems. The results suggest that due to the lack of effective electron conductive pathways along the NaO_2 surface, O_2 reduction (and evolution) reactions take place at the air electrode/electrolyte interface rather than on the NaO_2 surface. The poor electronic conductivity of NaO_2 may also contribute to the poor cycling performance seen in Na-O₂ cells. Enhancing the charge transport characteristics of the Na-O₂ discharge product by either doping or engineering the discharge products/air electrode interface is proposed as a potential research direction to increase the efficiency of Na-O₂ cells.

3.2. Chemical Composition of the Discharge Product in Na-O₂ Cells

3.2.1. Effect of Kinetics on the Composition of the Products

The discharge product of alkali metal-O₂ cells has an undeniable role on the electrochemical response of the cell.^[53,65] Both the chemical composition and morphology of the discharge products have been proven to play important roles on the charging overpotential and discharge capacity of the cells. As mentioned earlier, Li_2O_2 has been detected as the discharge product of Li-O₂ cells.^[3,66] For Na-O₂ cells however, there is still no agreement on the chemical composition of the discharge product. Predications based on the electrochemical studies conducted by Abraham^[32] determined that Na_2O_2 should be the major discharge product in Na-O₂ cells, however, a stable crystalline phase of NaO_2 with a low charging overpotential was detected as the discharge product of the cell by Hartmann et al.^[4,39,40] (Figure 6a). Formation of a crystalline superoxide phase was also confirmed using variety of analytical techniques including SEM-EDS, XRD and Raman. McCloskey et al.^[21] also measured the number of transferred electrons per consumed and evolved O_2 during the discharge and charge cycles of Na-O₂ cell using differential electrochemical mass spectrometry (DEMS) to be close to 1, indicating that the product of the cell is NaO_2 (Figure 6b). The superoxide-based products in this series of studies exhibited unprecedented low charge overpotential (≈ 0.1 V, Figure 6a and b) which in turn triggered a number of other studies on Na-O₂ battery system. In another study by Janek and Adelhelm et al.,^[40] the authors compared the thermodynamics of Li- and Na-O systems. Based on standard Gibbs free energy values for Na-O₂ system, the formation of peroxide phase is computed

Table 2. The calculated ionic and electronic conductivity values for NaO_2 , Na_2O_2 and Li_2O_2 . Adapted from ref. [54].

Compound	Ionic Conductivity ($S\ cm^{-1}$)	Electronic conductivity ($S\ cm^{-1}$)
NaO_2	$4 \times 10^{-9}/1 \times 10^{-10}$	1×10^{-19}
Na_2O_2	5×10^{-20}	1×10^{-20}
Li_2O_2	9×10^{-19}	5×10^{-20}

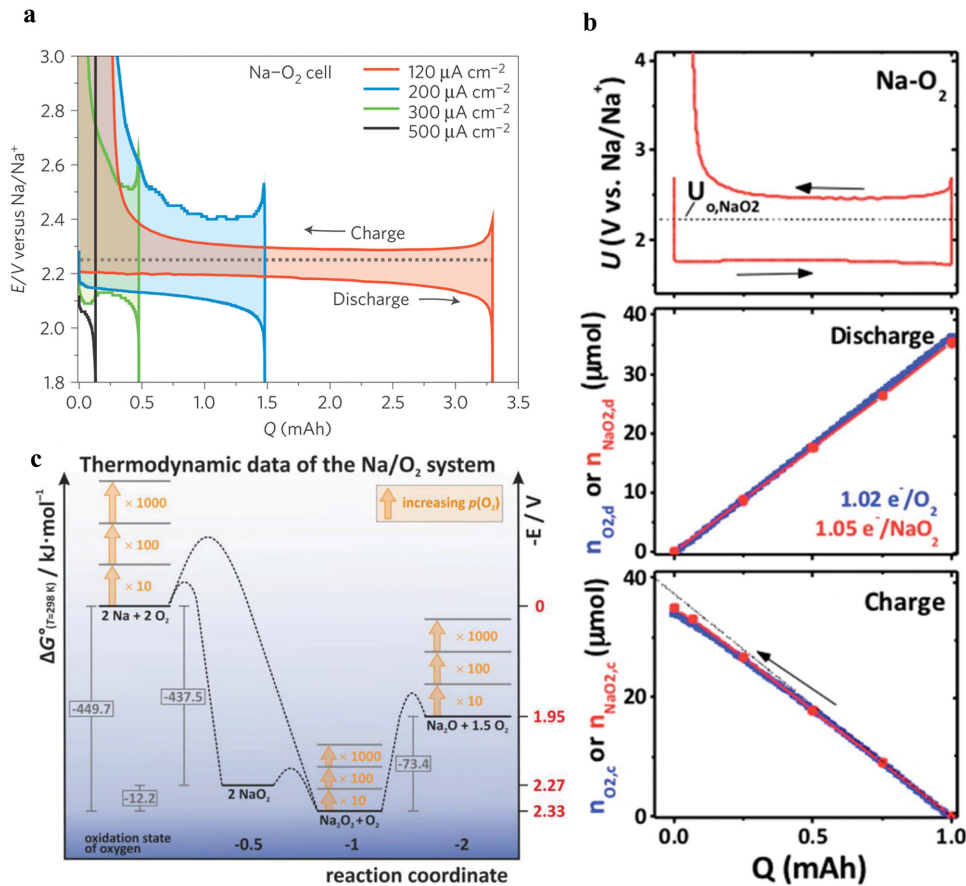


Figure 6. a) Discharge/charge cycles of Na-O₂ cells at various current densities. a) Reproduced with permission.^[4] Copyright 2012, Nature Publishing Group. b) Galvanostatic discharge/charge of a Na-O₂ cell (top); O₂ consumption, n_{O₂,d}, and NaO₂ formation, n_{NaO₂,d}, during discharge (middle); O₂ evolution, n_{O₂,c}, and NaO₂ oxidation, n_{NaO₂,c}, during charge (bottom) (the dashed black line is a 1 e⁻ process). 0.2 N NaOTf in DME were used as electrolytes and the cell was discharged and charged at 0.5 mA. b) Reproduced with permission.^[21] Copyright 2014, American Chemical Society. c) The thermodynamic data of Na-O₂ cell. c) Reproduced with permission.^[40] Copyright 2014, Wiley-VCH.

to be thermodynamically more favored over superoxide phase by only 12.2 kJ mol⁻¹ ($\Delta G_{\text{Na}_2\text{O}_2}^0 = -449.7$ kJ mol⁻¹; $\Delta G_{2\text{NaO}_2}^0 = -437.5$ kJ mol⁻¹, see also Figure 6c). Therefore, kinetic parameters are thought to play an important role in determining the discharge product of Na-O₂ cells. In the case of Li-O₂ cells, however, the superoxide phase is thermodynamically unstable and cannot be stabilized by kinetic factors, resulting in formation of Li₂O₂ as the discharge product.^[8,37,66,67]

Further, it is argued that the superoxide is the most stable product at elevated oxygen pressures, since the corresponding free enthalpy increase at higher oxygen pressures for the starting materials (2Na + 2O₂) as well as the peroxide products (Na₂O₂ + O₂), but remains untouched for the superoxide (2NaO₂, see also Figure 6c). However, different experimental results were obtained by Zhao et al.^[22] who examined Na-O₂ cells under 100% O₂ and 80/20 vol% of Ar/O₂ atmospheres. With the use of XRD, the product of the cell (using an ether-based electrolyte and vertically aligned CNT air electrode) was detected to be NaO₂ under both Ar/O₂ and pure O₂ atmospheres. Moreover, a mixture of Na₂O₂·2H₂O and NaOH was found under flowing atmospheres which has been related to the introduction of humidity through the flowing oxygen atmosphere. Preferred

formation of NaO₂ under reduced oxygen partial pressure reveals that oxygen pressure may play a more complex role in determining the outcome of the discharge product. It should also be noted that the aforementioned thermodynamic data was calculated based on a simplified assumption of gas phase reactions between pure reactant phases, a situation which is far from experimental conditions where the electrochemical reactions are taking place at the three-phase interface.

Other reports have indicated that Na₂O₂ is the discharge product of Na-O₂ cells. For instance, using FTIR and selected area electron diffraction (SEAD), Sun et al. found a mixture of Na₂O₂ and Na₂CO₃ as the discharge product of Na-O₂ cells using a carbonate-based electrolyte.^[6] The formation of carbonate-based complexes is likely due to the decomposition of carbonate-based electrolyte.^[13,56] Liu et al.^[15] also examined the product of Na-O₂ cell in 1,2-dimethoxyethane (DME)-based electrolyte by SAED and found Na₂O₂ as the major product. With the aid of the XRD data, hydrated forms of sodium peroxide (Na₂O₂·2H₂O) were discovered as a discharge product in Na-O₂ cells using ether-based electrolytes.^[17,18,22] Formation of both superoxide and peroxide phases as the product of Na-O₂ cells further highlights the impact of kinetic factors

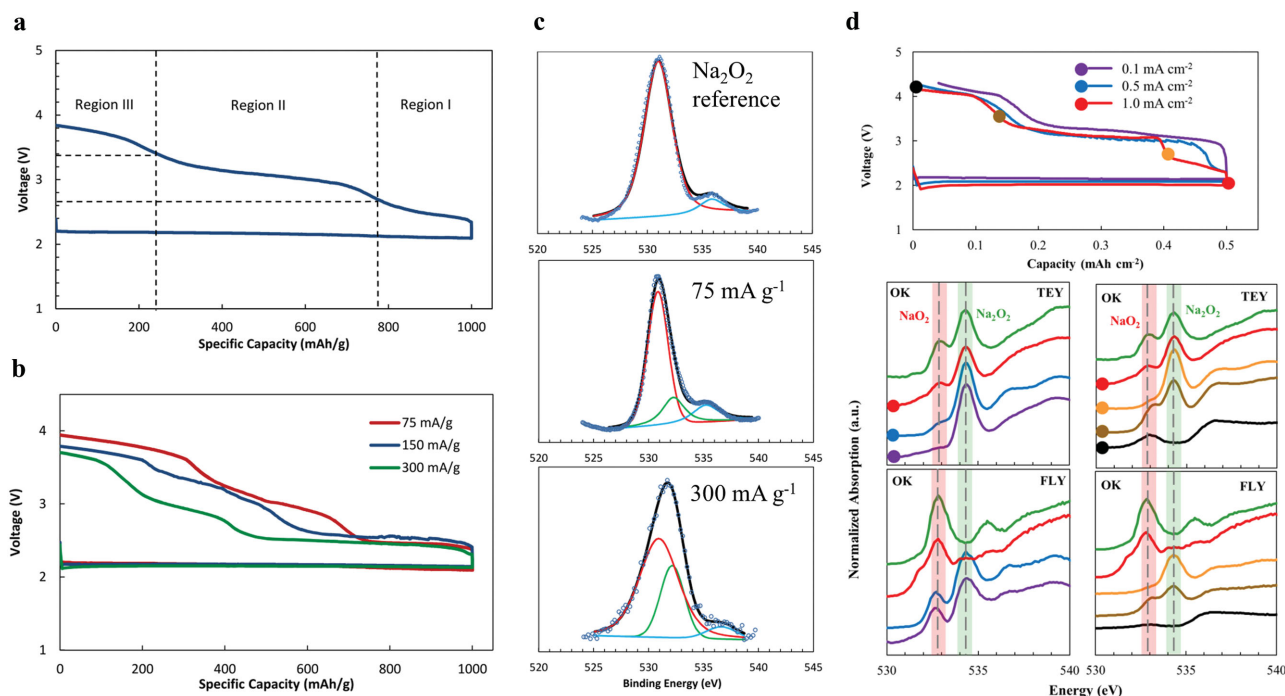


Figure 7. a) Limited discharge and charge curves of the Na-O₂ cell at current densities of 75 and 40 mA g⁻¹, respectively. b) Limited discharge and charge curves of Na-O₂ cells at different discharge current densities of 75, 150 and 300 mA g⁻¹ and a constant charge current density of 40 mA g⁻¹. c) Oxygen 1s spectra of reference sodium peroxide and discharge products resulted at current densities of 75 and 300 mA g⁻¹. a-c) Reproduced with permission.^[26] Copyright 2014, Royal Society of Chemistry. d) Restricted discharge and charge curves of Na-O₂ cell at different discharge current densities of 0.1, 0.5, and 1.0 mA cm⁻² and a constant charge current density of 0.1 mA cm⁻² (top); normalized O K-edge XANES spectra recorded under the TEY and FLY modes for the air electrodes discharged under different current densities of 0.1, 0.5, and 1.0 mA cm⁻² (left) and for the air electrodes charged to the various cutoff potentials of 2.75, 3.5, and 4.3 V (color coded) as well as the discharged air electrode and the standard Na₂O₂ sample (right). d) Reproduced with permission.^[30] Copyright 2015, American Chemical Society.

in determining the discharge product of Na-O₂ cell. We also studied the kinetics of Na-O₂ cells recently to further understand the reaction mechanism taking place.^[26] We employed a heat-treatment procedure on commercial carbon samples in the presence of corrosive gasses (NH₃ or CO₂) to produce a high surface area mesoporous carbon material. The synthesized high surface area carbon was then employed as an air electrode for Na-O₂ cells and several charging plateaus were found during the charge cycle (Figure 7a). A variety of analytical techniques including XRD, FTIR and Raman were used to evaluate the chemical composition of the discharge product in an attempt to understand the nature of the charging plateaus. It was found that both sodium peroxide and superoxide are produced as discharge products and decomposed with different overpotentials during the charge cycle. Interestingly, the discharge current density also affected the chemical composition of the product and consequently the charging overpotential of the cell (Figure 7b). XPS analysis of the discharge product formed under various discharge current densities revealed that the amount of superoxide-like product increases with increasing discharge current density (Figure 7c).

Furthermore, synchrotron-based X-ray absorption spectroscopy (XAS) was used to determine the chemical reaction mechanism of Na-O₂ cells employing a binder-free 3D-structured air electrode composed of vertically grown nitrogen doped carbon nanotubes on carbon paper (NCNT-CP).^[30] Compared

to our previous mechanism study,^[26] the binder-free nature of the 3D-structured air electrode eliminates any uncertainty regarding contribution from binder decomposition. The NCNT-CP air electrode exhibited multiple charging plateaus with variable capacities under several discharge current densities (Figure 7d). Using XAS, two distinct absorption peaks in the O K-edge X-ray absorption near edge structure (XANES) spectra of NCNT-CP air electrodes were observed, which can be attributed to sodium superoxide and peroxide. In addition, the absorption peak related to sodium superoxide exhibited a growing trend with increasing discharge current density (Figure 7d), indicating the preferred formation of sodium superoxide under elevated current densities. Furthermore, the chemical composition of surface and bulk components of the discharge products was compared by collecting the total electron yield (TEY) and the fluorescence yield (FLY) during photon absorption. Looking at both the TEY and FLY signal it is clear that the bulk of the discharge product is predominantly composed of a superoxide-like phase, while the surface consists of both superoxide and peroxide (Figure 7d). Reduced amount of superoxide-like phase in the superficial layer of the discharge product was related to the side reaction between the highly oxidative superoxide phase of the discharge product and the electrolyte.

The finding of our studies on Na-O₂ cell^[26,30] can be compared with kinetic studies conducted on Li-O₂ cells by Amin

and Curtiss et al.^[68,69] The authors provided analytical evidence toward the formation of a superoxide-like phase on a petroleum coke-based activated carbon (AC) with high surface area in an ether-based electrolyte.^[69] The Li-O₂ cell in this study showed two distinct charge plateaus at 3.2–3.5 V (for the first 40% of the charge cycle) and 4.2 (for the remaining 60% of the charge cycle). Although Li₂O₂ was detected using XRD on the discharged electrode, Raman spectroscopy showed characteristic peaks for both peroxide and superoxide-like phases. Density functional theory (DFT) calculations confirmed that the experimentally observed Raman peak is related to a superoxide-like phase adsorbed on the surface of a stoichiometric Li₂O₂ phase. The authors also used magnetic measurements to trace the formation and decomposition of superoxide-like phases during the discharge and charge cycles of the cell. A new magnetic transition was found following electrode discharge and subsequently disappears after charging the cell back to 3.7 V, confirming the formation and decomposition of a superoxide phase.

The same research group also reported on the reaction kinetics of Li-O₂ cells employing a similar high surface area air electrode.^[68] A similar two-step charging cycle was also observed, but the ratio between the lower and higher voltage plateaus decreased with increasing discharge capacity. The decrease in lower potential plateau was correlated to a decrease in the amount of superoxide due to the chemical disproportionation reaction of LiO₂ to Li₂O₂ through reaction (9). The authors then used the lower- and higher-potential charge plateaus as an indicator for relative amounts of LiO₂ and Li₂O₂ phases and found a first-order relation with a half-life of about 8 hours for the disproportionation of LiO₂. Another notable finding in this study is the correlation between relative amounts of superoxide phases and the discharge current density. Cells discharged at higher current densities exhibited higher charge capacity related to the lower-potential plateau. Two potential explanations are: I) lower discharge current densities provide longer time for disproportionation reaction and thus decrease the amount of superoxide phase; II) higher current densities result in higher LiO₂ nucleation due to increased rate of electron transfer. The authors also highlighted the role of the porous high surface area AC air electrode in providing an oxygen-rich environment with a large number of active sites for ORR. The dependency of charge overpotential in Li-O₂ cells on the discharge current density has also been reported by Scrosati et al.^[70,71] and Nazar et al.^[67] Similar plateaus at charge potentials lower than 3.5 V was observed by Nazar et al. which showed increasing trend of capacity with increase of discharge current density.

In order to have a comprehensive conclusion toward the most effective parameters in determining the reaction mechanism of alkali metal-O₂ cells, one should pay close attention to the experimental conditions affecting the electrochemical reaction occurring within the cell. A superficial comparison between studies on Na- and Li-O₂ cells reveals that a common point amongst these studies is the use of a highly porous air electrode with high surface area allowing for a large number of electrochemical active sites to be exposed. In addition, the amount of superoxide-like phase increases with increasing discharge current density in all cases (see also figure 7). Elevated discharge current densities results in faster consumption of dissolved oxygen at electrochemically active sites, which

accordingly leads to the oxygen depletion and decreased local oxygen concentration. Similarly, the increased surface area of the air electrode exposes a larger number of active reaction sites which can also be correlated to decreased local oxygen concentrations (since the amount of the electrolyte and hence the absolute amount of the dissolved oxygen into the electrolyte does not change grossly). As a result, it can be concluded that lower local concentrations of dissolved oxygen at electrochemically active sites results in the preferred formation of superoxide-like phases in alkali metal-O₂ cells. Such an interpretation on the effect of local oxygen concentration on the reaction mechanism of Na-O₂ cell is in accordance with the results obtained by Zhao et al.^[22] who found NaO₂ as the major product of the cell under reduced oxygen partial pressure.

The formation of cubic NaO₂ product on a relatively low surface area air electrode by Janek and Adelhelm^[4,40] can also be explained in a similar way. Due to the unique cell design containing a limited amount of oxygen employed in this series of studies, the electrochemical cells have been discharged under oxygen deficient environments. In addition, the relatively high discharge current densities used also contributed to faster consumption of dissolved oxygen, create oxygen deficient conditions. Such an explanation is in good agreement with the theoretical calculations by Lee et al.^[27] who employed the surface energies of sodium oxides with various crystalline structures to predict the equilibrium morphology of the discharge product in Na-O₂ cell. The cubic-shaped pyrite NaO₂ was predicted to be the preferred morphology of the cell under reducing conditions. It has been concluded therefore that the experimental conditions applied by Janek and Adelhelm^[4,40] was reducing and can also be obtained under oxygen deficient environments. Further, it has been mentioned that reducing conditions can also stem from higher oxygen consumption compared with its supply during the discharge cycle which can in turn be translated to higher discharge current density. The surface area of the air electrode and the amount of electrolyte employed are other experimental parameters that have been hinted by authors to contribute to the kinetics of discharge product formation. More kinetic studies are needed to truly understand the correlation between the kinetic parameters of Na-O₂ cell with the chemical composition of the discharge products. Such mechanism studies are especially important to control the charge overpotential of the cell.

3.2.2. Effect of Electrolyte on the Composition of the Products

A major hurdle for Li-O₂ batteries is electrolyte instability within the cells electrochemical window.^[11,12,29,72] Formation of parasitic side-products as a result of oxidative decomposition of the electrolyte components is believed to hinder the cyclability of the cell. A theoretical study by Viswanathan et al.^[73] suggested that the HOMO level and acid dissociation constant (pK_a) of the solvent is critical toward determining the chemical stability of Li-O₂ cell. An ideal solvent should have a low HOMO level and a high pK_a. However, a direct correlation was obtained between the HOMO level and pK_a for the most studied solvents. DME has been offered to be the most stable solvent among the available choices for Li-O₂ system based on its good compromise

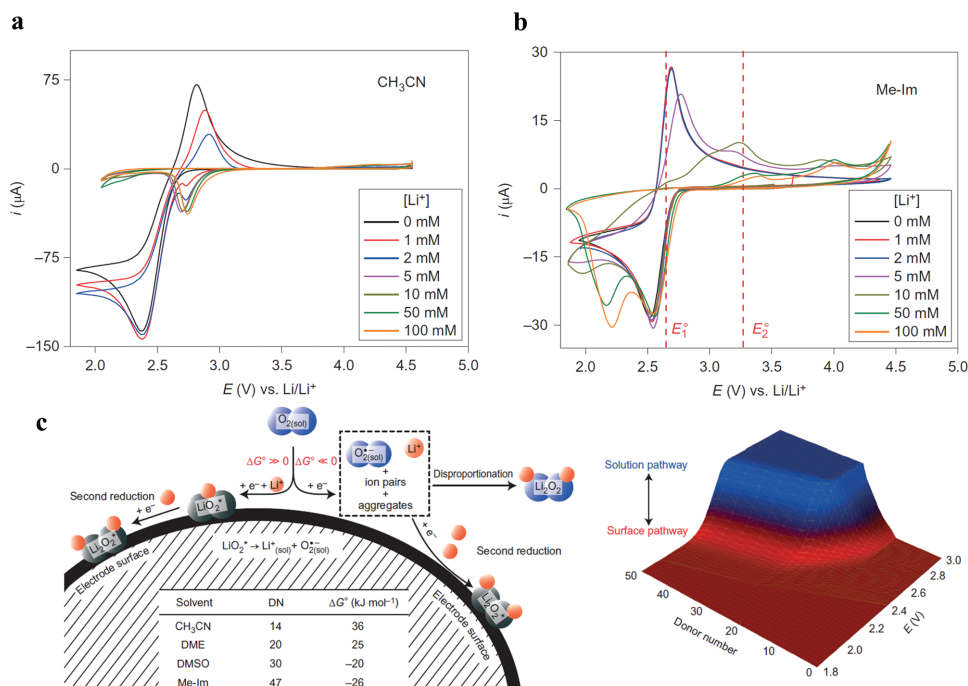


Figure 8. a, b) Cyclic voltammogram of a gold electrode in (a) CH₃CN and (b) Me-Im with various ratios of [Li⁺]:[TBA⁺]. The Li⁺ concentration is depicted on the plots, where the remaining concentrations to 100 mM are TBA⁺. The scan rate was 100 mV s⁻¹ and the anion was ClO₄⁻. c) Schematic of the O₂ reduction mechanism in an aprotic solvent containing Li⁺ showing the surface pathway followed when ΔG° < 0 (low DN) and the solution pathway followed when ΔG° > 0 (high DN). Plot at right corner shows the dominant pathway as a function of DN and potential. Reproduced with permission.^[75] Copyright 2014, Nature Publishing Group.

between the oxidative stability and H-abstraction. Nevertheless, McCloskey et al.^[72] showed that even DME is not thoroughly stable for practical applications.

The electrolyte may also alter the reaction mechanism of the cell. Abraham et al.^[74] initially studied the influence of the electrolyte solvent on the ORR mechanism in non-aqueous Li-O₂ cells. The solvents employed in this study were chosen to cover a range of donor numbers (DN), which is a quantitative measure of the Lewis basicity of cations. Using the large-diameter TBA⁺ cation, the authors observed a reversible one-electron redox reaction involving O₂/O₂⁻. In the presence of Li⁺ counter ion, however, more reduction steps were observed for O₂, implying that the Li⁺ ion has a decreased ability in stabilizing O₂²⁻, the initial product of ORR in non-aqueous electrolytes. Interestingly, it was found that electrolyte solvents with larger DN may influence the ORR kinetics in the presence of Li⁺ by stabilizing the O₂⁻ intermediate and hindering it from further reduction. Based on the HSAB theory, the Li⁺-solvent bond strength increases with the solvent's DN. As a result, the formed Li⁺-(solvent)_n complex in high-DN solvents acts as a moderately soft acid, resulting in a more effective interaction with the moderately soft O₂⁻ ion. On the other side, the Li⁺-(solvent)_n complex in low-DN solvents behaves as a hard acid due to the weak Li⁺-solvent bond, making a more effective interaction with O₂²⁻ ion which is a hard base. Consequently, high-DN solvents may stabilize the superoxide ion via making stronger Lewis acid-base complexes, while low-DN solvents facilitate the chemical or electrochemical reduction of O₂⁻ to O₂²⁻ ion.

More recently, Bruce et al.^[75] reinvestigated the role of solvents on the reaction mechanism of Li-O₂ cells using solvents with different DN. Using an approach similar to the study by Abraham et al.,^[74] the authors examined the electrochemical response of oxygen in the presence of both TBA⁺ and Li⁺ ions (Figure 8a and b). While a single one-electrode redox process was observed in the presence of TBA⁺ ion for all solvents, the electrochemical response of oxygen showed a strong dependency on the solvent's DN in the presence of Li⁺ ions. Low-DN solvents exhibited one reduction peak and one ill-defined oxidation peak at potentials over 4.0 V (Figure 8a). Interestingly, high-DN solvents demonstrated two consecutive reduction and two oxidation peaks at around 3.5 and 4.0 V (Figure 8b). The large potential separation between the reduction and oxidation peaks of oxygen has been related to the "EC" reaction mechanism in low-DN solvents. The single reduction peak in low-DN solvent is correlated to the electrochemical reduction of oxygen to O₂⁻. The produced O₂⁻ then chemically disproportionates to O₂²⁻, which correspondingly requires more positive potential for oxidation (>4 V). In high-DN solvents, however, the produced O₂⁻ ion is dissolved and stabilized into the solvent and is available at the electrode surface for further electrochemical reduction to O₂²⁻. Two reaction mechanisms have been proposed based on the different electrochemical responses for the ORR in low- and high-DN solvents (Figure 8c). In low-DN solvents, according to the authors, the produced LiO₂ adsorbs on the electrode surface where it quickly disproportionates to Li₂O₂. In high-DN solvents, however, LiO₂ initially dissolves into the electrolyte and then disproportionates to Li₂O₂ via a currently undefined

process. Furthermore, high-DN solvents demonstrate a considerable increase in discharge capacity compared to low-DN solvents. Higher discharge capacity in high-DN solvents has been correlated to the Li_2O_2 growth from the solution in contrast to its formation on the electrode surface in low-DN solvents.

Such a study related to the effect of the electrolyte solvent on the reaction mechanism found in Na- O_2 cells is still absent. However, it can be anticipated that Na- O_2 cells would show a more significant correlation between the electrochemical response of the cell and the electrolyte solvent, since the thermodynamic stability values of the sodium peroxide and superoxide are close (see also Figure 6e). It is expected that the chemical composition of the products in Na- O_2 cells can be precisely controlled with manipulating the kinetic parameters of the cell, including the electrolyte solvent. High-DN solvents may contribute to stabilize the superoxide phase and prevent disproportionation from occurring, which in turn results in lower charging overpotential in Na- O_2 cells. Based on the abovementioned criteria for a desired electrolyte solvent, identifying a high-DN solvent with low HOMO level and high $\text{p}K_a$ may greatly enhance the cyclability of the present Li- and Na- O_2 cells. It should be noted that an appropriate solvent must display compatibility with Li or Na metal anodes, high electrolyte salt and O_2 solubility, and high ionic conductivity. Finding such a desired electrolyte solvent would be less challenging in the case of Na- O_2 cell, since the charging overpotential of the cell is lowered to less than 3.5 V. So, a chemically stable solvent, with a relatively higher HOMO level, may also be beneficial for enhancing the Na- O_2 cell cyclability.

3.2.3. Effects of Chemical Composition of Discharge Product on the Charge Overpotential of Na- O_2 Cells

Amine and Curtiss et al.^[68,69] demonstrated analytical evidence regarding the presence of a lithium superoxide-like phase in Li- O_2 cells which were decomposed at a relatively low charging potential of 3.2–3.5 V. The authors attributed the low-potential charging plateau to the decomposition of a LiO_2 -like discharge product formed on $(\text{Li}_2\text{O}_2)_n$ clusters. Ceder et al.^[76] however, argued that the initial lower-potential charging step is correlated to the off-stoichiometric delithiation of Li_2O_2 to form local superoxide ion. The authors used ab initio computations to show that the formation of non-stoichiometric $\text{Li}_{2-x}\text{O}_2$ compounds out of Li_2O_2 discharge product is thermodynamically more favorable and requires only about 370 mV of overpotential. The formed off-stoichiometric states would then undergo further delithiation until finally decomposing into Li^+ and O_2 or O_2^- . Furthermore, the mobility of Li vacancy in Li_2O_2 is high enough to expect good electronic conductivity in off-stoichiometric $\text{Li}_{2-x}\text{O}_2$ phase.^[77–79] Higher electronic conductivity of the $\text{Li}_{2-x}\text{O}_2$ phase may also contribute in reducing the charging overpotential of the cell, since poor electrical conductivity of deposited Li_2O_2 at the air electrode/electrolyte interface is proposed to suppress charge transfer from occurring through the air electrode and increase the imposed potential during the charge cycle in order to overcome the charge transfer limitation.^[77,79,80]

In the case of Na- O_2 cells, however, an evident difference can be observed for the required charging overpotential. While

a low overpotential of less than 0.2 V has been obtained in some studies in which NaO_2 has been detected as the discharge product (Figure 6),^[4,21] a relatively high overpotential of more than 1 V has also been reported with Na_2O_2 as the main product.^[6,15,17] Similar to the Li- O_2 cell, a larger charging overpotential for Na_2O_2 might be related to the different electrochemical pathways during the discharge and charge cycles. Discharge reaction in Li- O_2 cell results in the formation of a LiO_2 intermediate which subsequently disproportionates to Li_2O_2 . On charging, however, Li_2O_2 directly decomposes to lithium and oxygen in a one-step electrochemical reaction.^[7] The different discharge and charge pathways reveal that the electrochemical reaction of the Li- O_2 cell might not involve a classic reversible redox couple.^[23] Meanwhile, other reports on Na- O_2 cells, exhibit more than one charge plateau with different overpotentials.^[18,22,23,26] In a previous study conducted by our group, we employed a variety of analytical techniques including a synchrotron-based XAS to determine the nature the discharge product at various charging plateaus.^[26,30] Based on this analysis, it was concluded that the superoxide-like product decomposes at a relatively lower overpotential compared to the peroxide-like product (see also Figure 7). In addition, a sodium deficient phase of sodium peroxide, with a general formula of $\text{Na}_{2-x}\text{O}_2$, was proposed to be formed as the product of Na- O_2 cells and can be decomposed at a middle overpotential.^[26]

Superoxide-like phases of lithium and sodium show lower charging overpotentials in both Li- and Na- O_2 cells. The observed lower overpotential might be related to the presence of a classic redox pair of O_2^-/O_2 . In the case of Na- O_2 cell, the higher radius of sodium ion contributes to stabilize the superoxide ion and form a solid sodium superoxide phase which has been detected as the major product of the cell by researchers.^[4,21] In addition, higher electrical conductivity of the oxygen-rich phases of lithium and sodium oxides may also contribute toward reducing the charging overpotential. Increased electrical and ionic conductivity of the oxygen-rich lithium peroxide phase may play an important role in decreasing the charging overpotential of the Li- O_2 cells. Regardless of the mechanism involved in the overpotential reduction, formation of the oxygen-rich oxide phases is beneficial in decreasing the charging overpotential for both Li- and Na- O_2 cells. Manipulating the kinetic parameters of the cells to enrich the oxygen-rich phases in the products of Li- and Na- O_2 cells can be considered as a research direction toward more energy-efficient cells. Future efforts should be devoted to truly understanding the role of kinetics parameters in the chemical composition of the discharge products of alkali metal- O_2 cells. However, based on literature available on Na- and Li- O_2 cells, it can be concluded that discharge products obtained under oxygen-deficient (reducing) conditions are more likely to be oxygen-rich.

4. Cyclability in Na- O_2 cell

4.1. Morphology of the Discharge Products

A variety of factors have been proposed to contribute in the relatively high charging overpotential and poor cycle life of the

Li-O₂ cell. Low electrical conductivity of the deposited Li₂O₂ at the electrode/electrolyte interface is thought to impose a large overpotential during the charging cycle in order to overcome the charge transfer limitation.^[77,79–81] In addition, formation of an insulating carbonate layer at the electrolyte/Li₂O₂ and Li₂O₂/carbonaceous air electrodes interfaces has been proven to contribute in high charging overpotential of the Li-O₂ cell, even in the relatively more stable electrolytes.^[9,13,14] However, a galvanostatic intermittent titration technique (GITT) study^[82] demonstrated that the equilibrium overpotential of Li-O₂ cells is close to zero, suggesting that the overpotential of the cell originates from a mass transfer limitation rather than the charge transfer one (at least under the low current densities). With the use of GITT, the authors were able to study the overpotential of the cell in both transient and steady-state modes. A zero open circuit voltage (OCV) hysteresis was observed between the equilibrium voltage of the discharge and charge of Li-O₂ cell during the GITT experiment with a 6 h relaxation time at 60 °C. The findings of this study also highlight the impact of product morphology on charging overpotential of the cell. The correlation between morphology of discharge product and charging overpotential is discussed in this section.

A number of studies have identified a crystalline cubic NaO₂ phase as the major discharge product in Na-O₂ cells (Figure 9a–c).^[4,19,22,40] Micrometer-sized discharge products of the cells in these studies exhibited a low charging overpotential. However, the Coulombic efficiency was lower than 100% in all cases, resulting in poor cycling performance of the cell. Electrical isolation of the products as a result of progression in decomposition process at the product/substrate interfaces might be responsible for poor cycling performance in these studies. However, other research studies have indicated that Na₂O₂ or its hydrated form (Na₂O₂·2H₂O) was the major discharge products (Figure 9d–f).^[16,18,83] Depending on the cells physicochemical conditions, a number of different morphologies have been observed for sodium peroxide discharge product. Meanwhile, a combination of NaO₂ and Na₂O₂ was also found in other studies (Figure 9g–i).^[23,26,30,84] A mixture of crystalline (cubic-like) and amorphous products can be recognized in SEM images, in accordance with the analytical characterization of the products. A variety of different physicochemical factors affect the morphology of products in metal-O₂ cells. Electrode/electrolyte interactions, electrolyte concentration, surface area of the air electrode, discharge current density and oxygen partial pressure are among the most effective factors.

A correlation between the charging overpotential and the morphology of the discharge products of Li- and Na-O₂ cell has been investigated in a few studies. Nazar et al.^[67] found that the morphology of the discharge product in Li-O₂ cells is influenced by discharge current density. The products morphology was changed from a crystalline toroid-shaped at lower current densities to an amorphous product at higher current densities (Figure 9m–o). The change in crystallinity with increasing discharge current density was also confirmed by XRD. More importantly, the change in product morphology was also accompanied by a corresponding decrease in charging overpotential. Formation of an amorphous deficient

phase of Li₂O₂ at higher discharge current densities has been proposed to be responsible for the reduction of charging overpotential.

A similar dependency of charging overpotential with discharge current density has also been observed for Na-O₂ cells (see Figure 7b). Further, a comparable conversion in the morphology of the discharge products was also found in our study on Na-O₂ cells.^[26] In the latter instance, the product morphology was correlated with an increase in the mesopore surface area of the electrode. While crystalline tablet-shaped particles were formed on low surface area air electrodes, nanometer thick films were observed in high surface area electrodes (Figure 9j–l). The conversion trend of product morphology in these two studies may seem contradictory at first, since the local discharge current density decreases with increasing active surface area. However, the local concentration of dissolved oxygen and/or metal ions at the electrochemical active sites exhibited a similar trend. The local concentration of the electrochemical active species at the air electrode surface decreases with an increase in both discharge current density and surface area of the air electrode. Low concentration of the electrochemical active species increases the local overpotential at active sites which in turn results in an accelerated nucleation process and formation of a deficient amorphous phase. It should also be noted that there should be a significant change in either the discharge current density or the air electrode surface area in order to recognize a distinguishable change in the morphology of the products. In the abovementioned studies for instance, the morphology of the cell products is monitored while the discharge current density and the specific surface area of the air electrode are increased by 20 and 17 times, respectively.

The correlation between morphology of Li-O₂ cell product and the discharge overpotential has been demonstrated in a study conducted by Shao-Horn and Thompson et al.^[85] A similar dependency of product morphology was also observed in this study, where large and crystalline Li₂O₂ particles were found after the discharge under a relatively low current density. However, an increased number of Li₂O₂ particles with smaller dimensions was obtained at higher current densities. The mechanism of nucleation and growth of discharge products is compared to the electrodeposition of metals on foreign substrates. Based on the Volmer-Weber island growth theory, higher discharge overpotential caused by a higher current density, results in more energetically accessible nucleation sites. Thus, the nucleation process exceeds the growth of the nuclease, forming an increased number of smaller particles. On the other side, a lower number of nucleation sites is energetically accessible at lower discharge overpotentials or lower current densities, resulting in exceeding the growth process and the formation of larger particles. A similar dependency of the product morphology on the discharge overpotential is also expected in the case of Na-O₂ cell. Furthermore, a nucleation-controlled regime may also result in the formation of deficient phases of lithium and sodium peroxide which is beneficial for both battery systems in terms of reducing the charging overpotential.

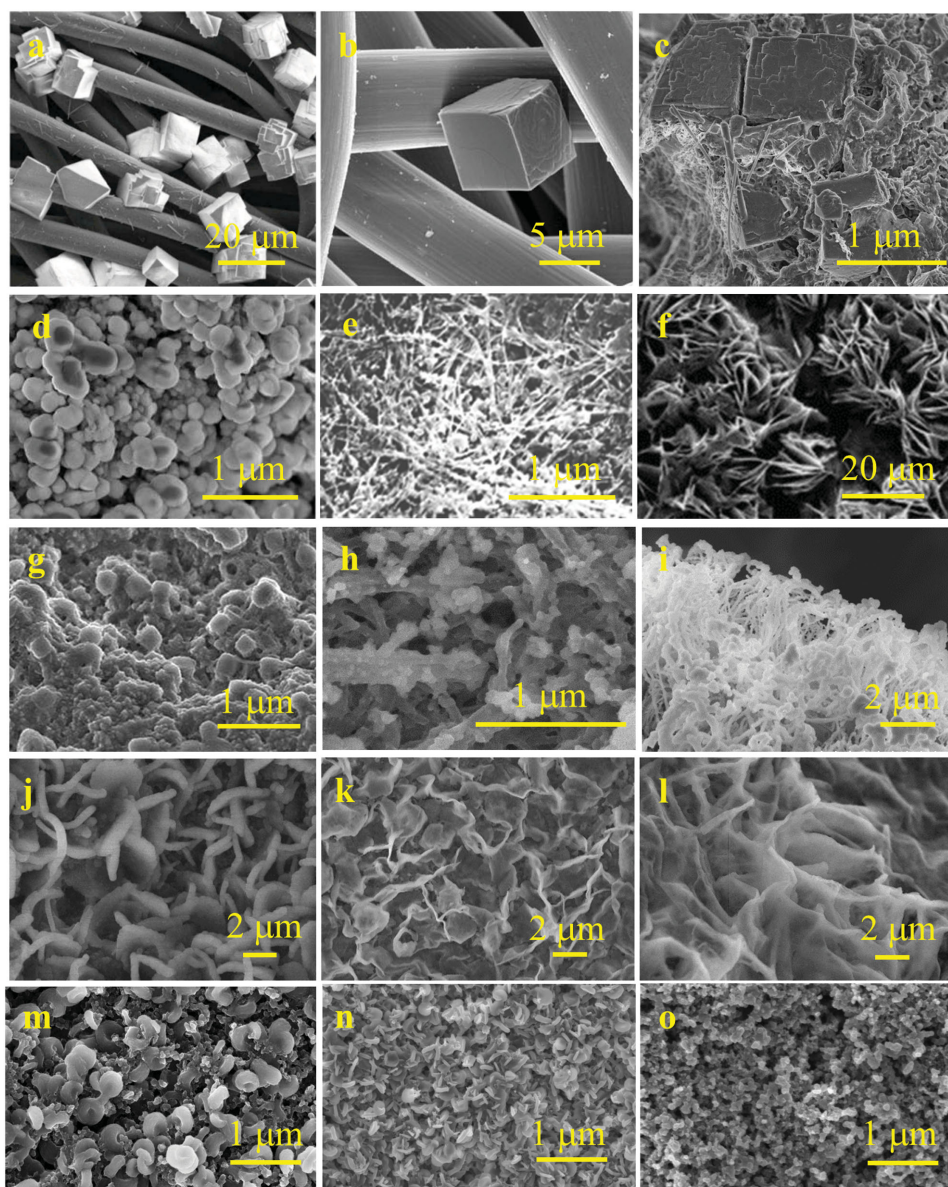


Figure 9. SEM images of the discharge products of Na-O₂ cell using (a, b) carbon fiber; (c) vertically aligned carbon nanotubes; (d) nitrogen-doped graphene nanosheets; (e) carbon nanotube paper; (f) NiCo₂O₄ nanosheets; (g) porous CaMnO₃; (h) nitrogen-doped carbon nanotubes; (i) nitrogen-doped carbon nanotubes on carbon paper air electrodes. j–l) Change in morphology of the discharge products of Na-O₂ cell using heat-treated carbon black with different specific surface area values of (j) 155.3 (k) 1053.5 (l) 1390.1 m² g⁻¹ as the air electrode. m–o) Change in morphology of the discharge products of Li-O₂ cell using Vulcan XC72 carbon black air electrode discharge under different current densities of (m) 5; (n) 25; and (o) 100 μA cm⁻². a) Reproduced with permission.^[19] Copyright 2013, Royal Society of Chemistry. b) Reproduced with permission.^[40] Copyright 2014, Wiley-VCH. c) Reproduced with permission.^[22] Copyright 2014, Royal Society of Chemistry. d) Reproduced with permission.^[16] Copyright 2013, Royal Society of Chemistry. e) Reproduced with permission.^[18] Copyright 2014, Elsevier. f) Reproduced with permission.^[83] Copyright 2014, Elsevier. g) Reproduced with permission.^[23] Copyright 2015, Royal Society of Chemistry. h) Reproduced with permission.^[84] Copyright 2015, Elsevier. i) Reproduced with permission.^[30] Copyright 2015, American Chemical Society. j–l) Reproduced with permission.^[26] Copyright 2014, Royal Society of Chemistry. m–o) Reproduced with permission.^[67] Copyright 2013, Royal Society of Chemistry.

4.2. Side Reactions

4.2.1. Parasitic Reactions

The chemistry of Na- and Li-O₂ cells was studied in a comparative study by McCloskey et al.^[21] Li-O₂ cells in this study exhibited an initial low charging overpotential which continually

increased to more than 4.5 V vs Li/Li⁺ in an ether-based electrolyte. Na-O₂ cells, however, displayed a low charging overpotential throughout most of the charge cycle with a sudden jump up to above 4 V vs Na/Na⁺. To learn more about the chemistry behind Na- and Li-O₂ cells, the authors examined the galvanostatic discharge/charge of Na- and Li-O₂ cells by means of DEMS. The number of electrons transferred per consumed and

evolved O_2 during the discharge and charge cycles of $Na-O_2$ cell was calculated to be close to 1, illustrating that the product of the cell is NaO_2 . In addition, the total parasitic side products formed during the discharge and charge cycles of the Na - and $Li-O_2$ cells was also measured based on the comparison of oxygen consumption and evolution to desired product formation (Li_2O_2 or NaO_2). $Na-O_2$ cell showed smaller deviation from the defined variables of average electrons consumed per O_2 , ratio of the amount of NaO_2 formed to amount of NaO_2 expected given the Coulometry, and ratio of O_2 evolved on charge to O_2 consumed on discharge. It was concluded then that $Na-O_2$ cell demonstrates “cleaner” chemistry compared to $Li-O_2$. Furthermore, it was found that less decomposition of the electrolyte/cathode occurs in the $Na-O_2$ cell and also that most parasitic decomposition in $Na-O_2$ cells occurs during the discharge rather than charge cycle (Figure 10a).

In contrast, side products in $Li-O_2$ cell (mainly lithium carbonates) continuously form during charge cycle of the cell and leads to a continually increasing charging overpotential. Nevertheless, the origin of the sudden overpotential increase around the end of charging cycle in $Na-O_2$ cell is not clear yet. The same electrochemical response was also observed in Hartmann’s studies.^[4,19] Either the accumulation of decomposition product on the air electrode surface or partial dissolution of NaO_2 into the electrolyte has been discussed as the potential reasons. However, a gradual increase of charging overpotential is expected to be seen in both cases. The mixed oxidation potential is expected to linearly increase with an increase in the side products/ NaO_2 ratio. In addition, a diffusion-controlled electrochemical response should be seen in the latter case. A more probable scenario could be considered based on the clues from direct observation of the air electrode after several discharge and charge cycles by Hartmann et al.^[19] Partially decomposed NaO_2 discharge product in deformed cubic shape could be seen on the air electrode surface after the cell cycling. It seems that progression of the decomposition process at the NaO_2 /air electrode interface sites cuts off the electrical contact to the remaining discharge particles, leading to a sudden jump in charging overpotential and limited cycling performance. This explanation is in perfect accordance with theoretical calculations performed on the electronic structure of NaO_2 by Arcelus et al.^[64] DFT calculations in the latter study revealed that the bulk, the extended (100) surface and $(NaO_2)_n$ clusters ($n = 4, 6$) exhibit band gaps larger than 2 eV. As a result, O_2 reduction, and consequently evolution reactions, take place at the electrolyte/air electrode interface rather than at the NaO_2 surface, leading to loss of electrical contact between NaO_2 particles and the air electrode during the charge cycle.

Furthermore, we also observed a continuous increase in the charging overpotential during consecutive discharge and charge cycles of $Na-O_2$ cells using NCNT-CP air electrode (Figure 10b).^[30] In contrast to the abovementioned studies, a gradual increase of charging overpotential was observed in our study. Analysis of the side products on the air electrode after electrochemical cycling revealed the presence of a carbonate-like phase as well as Na_2O_2 on the electrode surface (Figure 10c). Based on the electrochemical and analytical data, it was concluded that a carbonate-like parasitic side product is produced on high surface area air electrodes, mainly as a result

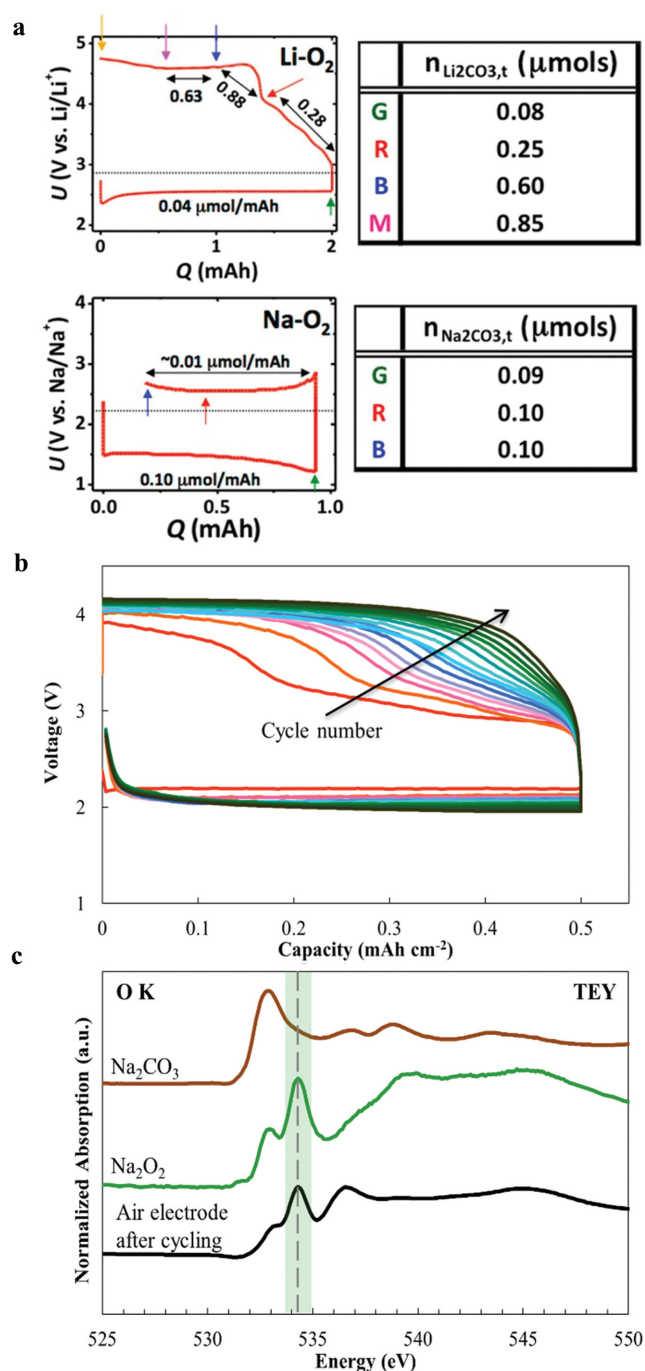


Figure 10. a) Galvanostatic discharge-charge curves of Li - and $Na-O_2$ cells, and total Li_2CO_3 and Na_2CO_3 formed as measured by CO_2 evolution from discharged and partially charged cathodes immersed in 3 M H_2SO_4 . The labels of the black arrows are the charge-normalized Li_2CO_3 or Na_2CO_3 (in $\mu\text{mol } Li_2CO_3$ or Na_2CO_3/mAh) over the corresponding regions. a) Reproduced with permission.^[21] Copyright 2014, American Chemical Society. b) Gradual increase of the charging overpotential during consecutive discharge and charge curves of $Na-O_2$ cell using NCNT-CP air electrode cycled between 1.8 and 4.3 V at a current density of 0.1 mA cm^{-2} . c) Normalized O K-edge XANES spectra recorded under the TEY mode for the cycled air electrode as well as the standard Na_2O_2 and Na_2CO_3 samples. b-c) Reproduced with permission.^[30] copyright 2015, American Chemical Society.

of decomposition occurring between the oxidative discharge product and the electrolyte. Accumulation of this insulating side product on the air electrode surface imposes an increasing overpotential to the cell during consecutive discharge/charge cycles and prevents complete decomposition of the discharge products. Even though Na-O₂ cells undergoes less chemical and electrochemical decomposition reactions compared to Li-O₂ counterparts during the first discharge and charge cycle according to McCloskey et al.,^[21] the formation and accumulation of carbonate-based parasitic side products on high surface area air electrodes and during consecutive discharge and charge cycles would be considerable. It is safe to say that the quantity of the parasitic products in Na-O₂ cell is lower than that of Li-O₂ due to the higher thermodynamic stability of NaO₂ phase compared to LiO₂. However, formation and accumulation of insulating side products as a result of the decomposition reaction between highly oxidative discharge products and the electrolyte is believed to be responsible for the limited cycle life observed for both cells.

4.2.2. Reactions Involving Carbon Dioxide

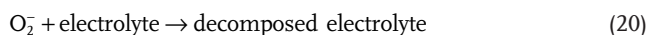
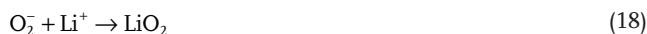
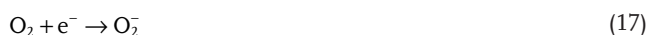
Formation of carbonates through parasitic reactions in Li- and Na-O₂ cells is unfavorable for both cells due to the high decomposition potential of carbonate-based products. Carbonates have been known to form as a result of the reactions involving the oxidation of solvents^[56] and carbon cathodes^[13] as well as the chemical/electrochemical reactions between LiO_x/NaO_x with CO₂. Although the influence of CO₂ on the Li/Na-O₂ cells with pure oxygen as the positive electrode material might be ruled out, it should be taken into consideration when ambient air is directly used as oxygen source for practical Li/Na-“air” batteries. These minor components in air may bring various side reactions, which can possibly influence the electrochemical reaction route and affect the performance of the metal-air batteries.

Gowda et al.^[86] investigated the effect of CO₂ contamination in Li-O₂ cell using DME electrolyte for the first time. This study compared the electrochemical behavior of cells using pure O₂, pure CO₂ and 10:90 CO₂/O₂ mixture gas. They observed a 2 e⁻/O₂ electrochemical process regardless of the presence or absence of CO₂, representing the formation of Li₂O₂ during the discharge cycle of the cells. In presence of CO₂, however, a spontaneous chemical reaction between Li₂O₂ and CO₂ resulted in formation of Li₂CO₃. Moreover, metallic Li anode was also reported to react with CO₂ and O₂ to form Li₂CO₃. The corresponding reactions are summarized as follows:^[86]



The presence of Li₂CO₃ in the discharge product caused a significant increase to the overpotential required for releasing CO₂ during the charging process. Accordingly, the authors concluded it is essential to completely remove CO₂ from air to create a working rechargeable Li-air battery.

Later, Lim et al.^[87] extended the study on the effect of CO₂ to a wider range of solvents combining both quantum mechanical calculations and experimental evidences. They revealed the reaction chemistry of Li-O₂ cell involving CO₂ during the initial stage of battery operation. It was found that the electrolyte solvation effect plays a critical role in alternating the reaction route at the initial complex formation (ICF) step. The proposed ICF processes involved is based on the following reaction scheme:^[87]



The authors stated that the potential energy surface plays a critical role in the formation of the final discharge product in the Li-air cell. Low dielectric solvents like DME were predicted to lead to the formation of Li₂O₂, while high dielectric solvents such as DMSO will result in the electrochemical activation of CO₂ to directly form Li₂CO₃ (Figure 11a). The authors also determined the chemical compositions of discharge products of Li-(9:1 O₂/CO₂) cell with DMSO and DME electrolytes to be only crystallized Li₂CO₃ and amorphous Li₂O₂-Li₂CO₃ mixtures, respectively, which is consistent with theoretical calculations. The GITT measurements of the Li-O₂ and Li-O₂/CO₂ batteries clearly displayed the differences between their electrochemical reaction mechanisms. Interestingly, Li-O₂/CO₂ cell with DMSO electrolyte was found to be highly reversible with Li₂CO₃ discharge products, implying the possibility of building Li-O₂/CO₂ batteries with high dielectric electrolytes.

The poisoning effect of CO₂ on (1–100) faced Li₂O₂ was investigated using DFT calculations by Mekonnen et al.^[88] This facet was reported to possess suitable nucleation sites toward low overpotential growth of Li₂O₂.^[89] It was found that CO₂ preferentially binds at step valley site at the Li₂O₂ surface and alters its growth mechanism. Even at a low concentration of 1%, CO₂ will severely block surface nucleation sites and result in a larger capacity as well as increased overpotential. Lu et al. carried out *in situ* XPS experiments on Li-O₂/CO₂ cell and observed the formation of carbonate which was not fully decomposed during charging.^[90] Nevertheless, the role of Li₂CO₃ on the rechargeability of the Li-O₂/air batteries can be more complicated than expected. Zhang and Zhou demonstrated a highly reversible Li-air battery with multi-layer electrolytes and a gel single-walled carbon nanotubes/ionic liquid (IL) cathode. Li₂CO₃ was found to be the discharge product and believed to result from the reaction between Li₂O₂, H₂O and CO₂.^[91] Also, increasing interest has been drawn toward the development of reversible Li-CO₂/O₂ batteries. It is also worth noting that a Li-pure CO₂ battery does not deliver negligible capacity compared to CO₂/O₂ mixture gas with EC:DEC^[92]

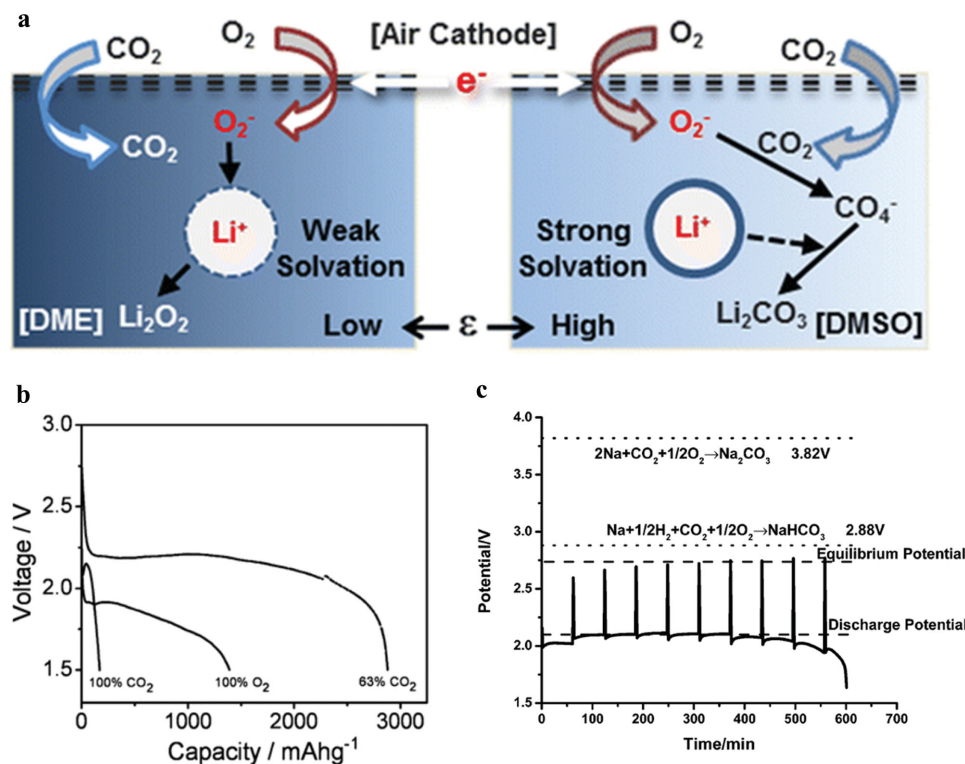


Figure 11. Effect of CO₂ on the electrochemical behavior of Na-O₂ batteries. a) Schematic graph of OER reaction pathways of a Li-O₂ battery in the presence of CO₂ with DME and DMSO electrolytes summarized from theoretical calculation and experimental evidence. a) Reproduced with permission.^[87] Copyright 2013, American Chemical Society. b) Comparison of discharge profiles of Na-CO₂, Na-O₂, and Na-CO₂/O₂ cells with tetraglyme electrolyte. b) Reproduced with permission.^[94] Copyright 2013, Elsevier. c) GITT discharge profile of Na-CO₂/O₂ cell with propylene carbonate electrolyte with the dotted lines indicating the theoretical potentials. c) Reproduced with permission.^[95] Copyright 2014, Royal Society of Chemistry.

or DME^[86] electrolytes, but the cells with mixed CO₂/O₂ gas exhibited a 1.5 to 2.9 fold increase in capacity compared to pure oxygen. However the Li-pure CO₂ battery is found to be highly reversible with TEGDME electrolyte as well as the Li-O₂/CO₂ one.^[93] These results imply the complex role of CO₂ in Li-air batteries, which needs to be taken into careful consideration for the practical cells.

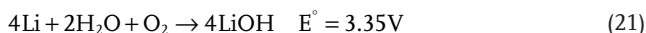
The impact of CO₂ on Na-air batteries was investigated by Archer and co-workers with IL, TEGDME, and PC electrolytes^[94,95] and its reaction mechanism was proven to be even more complicated. As shown in Figure 11b, Na-CO₂/O₂ batteries with TEGDME present a 2.5 fold increase in capacity compared to the battery using pure O₂, while the Na-pure CO₂ batteries displayed decreased capacity. Na₂CO₃ and Na₂C₂O₄ were both detected in the discharge product for TEGDME electrolyte, while Na₂C₂O₄ is the major product with an IL electrolyte. In contrast, NaHCO₃ was found to be formed in the discharge product of Na-CO₂/O₂ batteries with PC electrolytes (Figure 12c). Such contrast between the electrochemical behavior and discharge products of Na-CO₂/O₂ batteries with different electrolytes may be attributed to the difference between solvation effect of the electrolyte and stability of lithium/sodium salts according to HSAB theory as mentioned above. However, further theoretical calculations are still needed to address the insufficient understanding of the effect of CO₂ on Na-air batteries in future.

4.2.3. Humidity Effect

Similar to CO₂, water is another non-negligible component in air that has underestimated influence on Li- and Na-air batteries. Unlike CO₂, H₂O mainly exists as liquid phase at SATP. Its maximum concentration in gas is determined by saturation water vapor pressure under certain temperature and pressure. Therefore, the concentration of water in air is often expressed by the ratio of the actual water vapor pressure to the saturation water vapor pressure at the same condition and referred to as relative humidity (RH). The saturation water concentration in air at SATP is around 3%, which is around 75 times higher than the normal concentration of CO₂ in atmosphere (~0.04%), whose impact should certainly be taken into serious consideration in Li/Na-air batteries. Although one may simply assume that water will be fatal to a Li/Na-air battery, due to its chemical reactivity toward lithium and sodium and their (super, per)oxides, its role in these batteries has been proven to be more complex and critical than expected.

Meini et al. compared the electrochemical behavior of Li-O₂ batteries with and without of water in the electrolyte with an improved cell design for the first time.^[96] It was surprising to observe that a cell with 1000 ppm of water exhibited a capacity increase 2.8 times than that of a water-free cell. When the authors purged the O₂ with water vapor into the cell, it demonstrated an overwhelming large capacity of around 14 times than

that of the water-free one. A ~50 mV higher increased voltage output was also observed for the water-contaminated cell comparing to the dry one. Therefore, the authors proposed the following alternation reaction mechanism:^[96]



which is 40 mV higher than the potential corresponding to the formation of Li_2O_2 (Equation (8)), and suggested that the capacity of Li- O_2 batteries should be carefully calibrated by taking the impact of water into consideration.

This phenomenon that trace amount of water can significantly enhance the discharge capacity of Li- O_2 batteries has been also supported by studies conducted by other researchers.^[97,98] Guo et al. studied the influence of RH on the performance of Li- O_2 batteries in detail.^[97] They found that the cell ran under O_2 with 15% RH showed twice of the capacity than that with dry O_2 . However, any efforts in further increasing the RH to 50% resulted in decreased electrochemical performance. IR and XRD analysis concluded that Li_2O_2 , LiOH and Li_2CO_3 are the major discharge products formed under wet environments. Interestingly, it is worthy to note that even under wet conditions, Li- O_2 batteries were found to be reversible and maintain 30–50 cycles with a cut-off capacity of 1000 mAh g^{-1} at a current density of 200 mA g^{-1} . This indicates that the impact of water on Li- O_2 batteries can be subtle and therefore be easily underestimated and ignored. Cho et al. focused on the influence of water vapor on the metallic Li anode and reported that water can penetrate the cell and directly react with Li to form LiOH and release H_2 , which was responsible to the failure of the cell.^[98]

Recently, understanding of the role of water in Li- O_2 batteries has been further deepen. It was reported that the formation and growth of large Li_2O_2 toroids can be surprisingly promoted by adding water to the electrolyte mixture.^[99,100] It was reported in one study that no LiOH was detected in cathodes discharged in electrolytes with up to 1% of water.^[100] This unanticipated behavior of Li- O_2 batteries is believed to be related to the sophisticated chemistry and stability of Li_2O_2 against H_2O . Gasteiger and co-workers proposed the formation of Li_2O_2 in the presence of water may involve the recrystallization reaction route of Li_2O_2 .^[100,101]

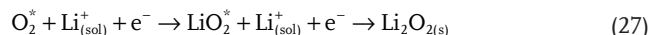


where H_2O_2 may originate as a result of the following reactions:



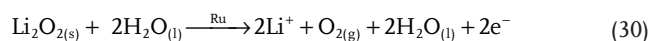
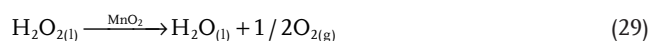
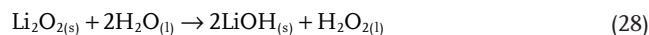
Aetukuri et al. reported that the promotion effect of water on the discharge capacity of Li-air batteries roots in the alternation of surface reaction mechanism to a solvent dissolution of

superoxide anion O_2^- as a redox mediator.^[99] Water, as a high AN solvent, is believed to contribute in the stabilization of O_2^- , and thus promote the dissolution for LiO_2^* into Li^+ (sol) and O_2^- (sol). The following reactions then take place:



As a result, Li_2O_2 is formed as the final product of Li-air batteries in the presence of water. Nonetheless, the authors suggest that water cannot be considered as a good additive, since it will increase parasitic reactions in the cell.

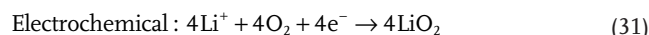
More recently, a new strategy to reduce the charging overpotentials of Li- O_2 batteries by intentional formation and decomposition of LiOH produced in the presence of water has been also proposed. Li et al.^[102] reported that adding 120 ppm of water to DMSO-based electrolyte results in significant reduction of the charge overpotential to 0.21 V in Li- O_2 cell with a Ru/MnO₂/Super P air electrode, leading a discharge/charge potential gap of only 0.32 V and a superior cycling life of 200 cycles. The synergistic effect of Ru/MnO₂/Super P catalyst during the charge cycle was proposed to undergo the following reaction:^[102]



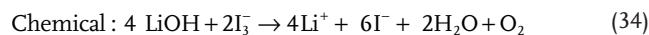
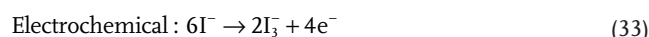
The authors also noted that further increasing the amount of water (281 ppm) leads to a shortened charge plateau with increased charging potential. Higher Nernstian potential resulted from increased concentration of H_2O around pre-formed LiOH is suggested as the possible reason.^[102]

Similarly, Liu et al. also reported that dissolved LiI catalyst can also act as a soluble catalyst to promote the efficient removal of LiOH.^[103]

Discharge:



Charge:



A low potential gap of 0.2 V between discharge and charge plateaus was reported by combining an rGO air electrode and LiI containing LiTFSI/DME electrolyte.^[103] Both of the above studies provide insight into the use of water as a chemical reagent for converting $\text{LiO}_2/\text{Li}_2\text{O}_2$ to LiOH in effort to reduce the overpotential of OER. These new findings are important in terms of both fundamental understanding and possible practical applications of Li- O_2 batteries.

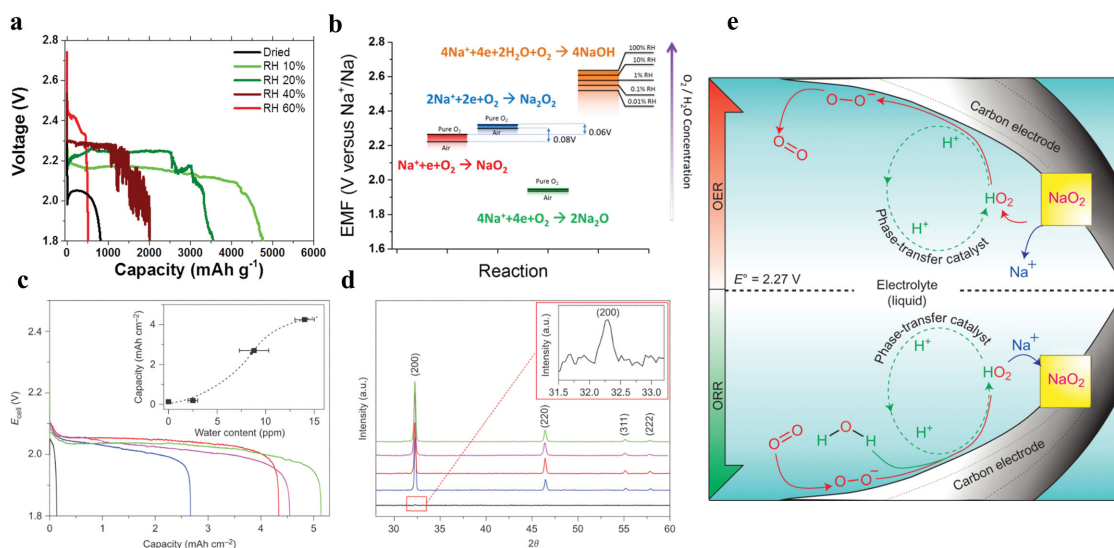
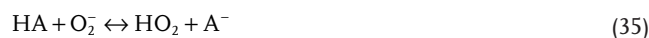


Figure 12. Effect of water on the electrochemical response of Na-O₂ batteries. a) Discharge curves of Na-air batteries under dry and ambient humid air with relative humidity of 10% to 60%. b) Reproduced with permission.^[96] Copyright 2012, The Electrochemical Society. c) First discharge curves of Na-O₂ cells using water-free and water-containing NaOTf salts and (inset) evolution of cell capacity toward water contents ranging from 0 to 14 ppm. d) XRD patterns of the discharged cathodes: black for dry pure NaOTf, blue for with 8 ppm water added, red for pure NaOTf with 14 ppm water, magenta for with 10 ppm anhydrous benzoic acid added, green for with 10 ppm anhydrous acetic acid added. e) Schematic graphs of the role of proton playing in ORR and OER processes of Na-O₂ cells as phase-transfer catalyst. c-e) Reproduced with permission.^[105] Copyright 2015, Nature Publishing Group.

Analogously, revealing the role of water in a Na-O₂ cell can be expected to be equally essential to Li ones. Our group has systematically investigated the composition of discharge product in Na-air batteries under different RHs recently.^[104] We examined the electrochemical performance of the Na-air batteries under dry environments and RH ranging from 10–60% (Figure 12a), and identified the chemical composition of the corresponding discharge products under different RHs by their XRD patterns, FT-IR spectra and SEM images. Based on these experimental evidences, we have shown that the presence of water will alternate the reactions in Na-air batteries both chemically and electrochemically, which is also supported by thermodynamic calculations (Figure 12b). Na-air batteries are much more sensitive to water than Li ones. Although the cells presented increased discharge capacities under high RH, they were found to be totally irreversible and broke down during the first charge/discharge cycle. The discharge products of Na-air batteries under different RHs were found ranging from sodium superoxide and peroxide to hydroxides and carbonates, even with the same air electrode composition and cell configuration. These results might contribute toward clarifying the inconsistencies in the studies on Na-air batteries where different discharge products are observed. Besides, we also reported the releasing of liquid phase water from decomposing NaOH during the charge process, which is the reason for failure in Na-air batteries.

Nazar and co-workers investigated the critical role of protons in Na-O₂ batteries by comparing home-made water-free electrolyte salts with commercially available ones.^[105] They showed that trace amounts of water in the electrolyte solution dramatically increases the capacities of cells (Figure 12c),

as often introduced by commercial electrolyte salts and resulted in approximately 10 ppm H₂O in the electrolytes. More interestingly, they have shown that other proton donors like anhydrous acetic acid and benzoic acid could perform a similar role to promote the growth of cubic NaO₂. NaO₂ was confirmed to be the only discharge product by XRD with electrolytes containing up to 14 ppm water or acids (Figure 12d). Accordingly, the reaction mechanisms were proposed as below:^[105]



where HA represents a weak acid. These weak acids play a role of phase-transfer catalyst and a low concentration of these species are proven to be essential to enable sufficient performance of Na-O₂ batteries (Figure 12e).

Ortiz-Vitoriano et al. reported that ambient exposure of discharged air electrode caused the transformation of NaO₂ in discharged electrode to Na₂O₂·2H₂O based on Raman and XRD evidences.^[31] In contrast, they stated that based on XRD results, only pure-phase NaO₂ was found to be the discharge product even at high concentrations of water electrolyte (6000 ppm). It was also noted by the authors that the actual water content in the electrolyte could be consumed by its reaction with the Na negative electrode. These results are consistent with the previous study by Zhao et al.,^[22] who found that the discharge products of Na-air batteries contained NaO₂ under static oxygen environment and Na₂O₂·2H₂O under flowing oxygen gas. They

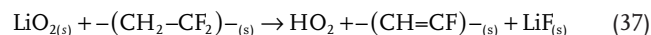
also attributed the formation of $\text{Na}_2\text{O}_2 \cdot 2\text{H}_2\text{O}$ to the water content in the oxygen gas.

It can be inferred that water contamination in the gas input has a severe impact on the electrochemical performance of Na-air batteries. This can be attributed to the continuous supply of water from the flowing gas. Ortiz-Vitoriano et al. calculated the amount of water required to react with NaO_2 and produce $\text{Na}_2\text{O}_2 \cdot 2\text{H}_2\text{O}$ in a cell with a total discharge capacity of 1 mAh to be 3.73×10^{-5} mol.^[31] The concentration of this amount of water in a typical 120 μl of electrolyte in the cell equals to around 6400 ppm. Here in this review, we can also simply estimate the content of humidity in air at SATP by ideal gas law $PV = nRT$, where p is pressure, V is volume, n is mols of gas, R is gas constant, and T is absolute temperature in kelvin. The corresponding value of water vapor concentration in ambient air of 100% RH at room temperature (25°C) can be calculated to be approximately 1.28×10^{-6} mol mL^{-1} . This literally means that approximately 60 mL of air with RH of 50% at SATP is theoretically capable of providing adequate water to decompose the same amount (1 mAh) of NaO_2 as above. This comparison can provide a preliminary understanding over the influence of water from gas input, considering a typical flow rate of several or tens of scm (mL min^{-1}) during the metal-air battery testing.

In summary, all the above studies strongly indicate the importance role of water from both electrolyte and gas sources, which can be easily ignored but may contribute in drastically different electrochemical behaviors and rechargeability of the Li/Na- O_2 batteries. We believe that this aspect should be carefully considered by the researchers moving from Li- O_2 to Na- O_2 batteries.

4.2.4. Binder

Binder is considered as another important component in the composition of air electrodes, which is generally a polymer and commonly used in the cathodes of Li/Na- O_2 batteries to integrate and hold the catalyst, conductive carbon, and supporting substrate together. Regardless of self-standing binder-free air electrodes, binders are widely used for powder-based air electrodes. Polyvinylidene fluoride (PVDF) has been the most common choice adopted for metal- O_2 batteries, as it is also one of the most universally used binders for Li-ion batteries (LIBs). However, the role of binders in metal- O_2 batteries can be equally vital compared to other components in the cell. Nazar and co-workers noticed the instability of PVDF binder towards superoxide species for the first time, and proposed the following decomposition route:^[106]



The formed HO_2 subsequently disproportionates to H_2O_2 or H_2O together with O_2 . This finding stimulates the urgent demand to search for an ideal binder for metal-oxygen batteries. Nasybulin et al. carried out a labour-intensive effort to screen the stability and reactivity of various binders.^[107] Eleven types of polymers were chosen to be dissolved in different solvents and mixed with Ketjenblack (KB) carbon black to fabricate air electrodes. Their chemical stabilities against peroxide and

superoxide were examined by ball-milling the polymers with Li_2O_2 or KO_2 , respectively, while the products were identified by XPS and XRD. A similar study was also carried out by Shao-Horn et al.^[108] FT-IR, UV-VIS absorption, and NMR characterizations were adopted for their study. In summary, the results and conclusions on the stability of the binders against superoxide and peroxide formation from these studies are listed in Table 3. It can be concluded that the functional groups on the backbone chain of the polymers are generally vulnerable to nucleophilic substitution attacking of O_2^- and O_2^{2-} . The decomposition of binders can not only lead to the disintegration of the air electrode by losing sticking force, but also may form various side products from the decomposition reactions (e.g., H_2O), which could possibly participate in further side chemical/electrochemical reactions with discharge products, metal Li/Na anodes, and/or electrolytes to cause the failure of the cells. Therefore, a stabilized binder toward superoxide/peroxide can be crucial toward developing long-life rechargeable Na-air batteries. As a conclusion summarized from Table 3, polyethylene (PE), polypropylene (PP), and fully fluorinated polymers (e.g., polytetrafluoroethylene (PTFE) and Nafion) are believed to be the most stable binders for these batteries. On one hand, novel polymer(s) have been also designed and tested for Li- O_2 batteries (e.g., polyisobutylene (PIB)).^[109] On the other hand, a binder-free design of air electrode may also be an alternative solution to this difficulty.^[30]

However, it should be noted that the abovementioned experiments on the stability of various polymers are generally carried out in a chemical (liquid-phase) or physical (ball-milling) environment. The effect of binder (decomposition) on a practical electrochemical cell may be more intricate than what have been suggested by their chemical reactivities. For example, it was reported that although PE was found to be the most stable polymer against superoxide/peroxide, the Li- O_2 battery with PE binder did not exhibited significantly prolonged cycling life compared to a cell made with PVDF binder (27 cycles versus 26 cycles).^[107] The authors attributed this phenomenon to an initial passivation stage of the binder by electrolyte decomposition. On the other hand, Shao-Horn and co-workers reported the decomposition of poly(ethylene oxide) (PEO) during charging to be much more severer in the presence of O_2 than under Ar.^[110] These studies suggest the necessity for the investigation of binders toward practical air cells. Nonetheless, the systematic experimental identification on the effect of binders for a practical Na- O_2 battery is still not presented. Our group has planned to address this aspect experimentally in the near future.

5. Air Electrode Design

5.1. Carbon-Based Air Electrodes

The gas diffusion electrode plays a fundamental role in metal- O_2 cells. The air electrode in these cells serves as a diffusing medium for the positive active material (oxygen) into the cell. This electrode must also provide adequate surface area for the accumulation of insoluble discharge product produced during electrochemical cycling. As a result, the final performance of the cell is strongly dependent on the efficiency of the air

Table 3. An overall summary of the reported stability of polymer binders versus superoxide and peroxide.

Binder/Polymer	Stability against O_2^-	Stability against O_2^{2-}	Decompose Product	Reference
PVDF	No	No	$K(HF_2)$ (KO_2)	[107]
PVDF	No	–	HO_2 ; $-(CH=CF)-$; LiF (LiO_2)	[106]
PVDF	–	No	–	[108]
PVDF-HFP	–	No	–	[108]
PEO	No	–	K_2CO_3 (KO_2)	[107]
PEO	–	Possible crosslink	–	[108]
PTFE	Yes	Yes	–	[107]
PTFE	–	Yes	–	[108]
Nafion	–	Yes	–	[108]
CMC	No	–	K_2CO_3 (KO_2)	[107]
PP	Yes	Yes	–	[107]
PE	Yes	Yes	–	[107]
PVP	No	–	K_2CO_3 (KO_2)	[107]
PVP	–	No	–	[108]
PS	No	–	K_2CO_{23} (KO_2)	[107]
PAN	No	–	KCN (KO_2)	[107]
PAN	–	No	$-C=N$; $-C=C-N$ (Li_2O_2)	[108]
PVC	No	–	$LiCl$	[107]
PVC	–	No	–	[108]
PMMA	No	–	K_2CO_3 (KO_2)	[107]
PMMA	–	Yes	–	[108]
PIB	Yes	Yes	–	[109]

electrode. An ideal air electrode should possess proper porous structure with an appropriate pore volume and pore size distribution. The porous structure is responsible for oxygen diffusion into the positive electrode material, formation and storage of the discharge products and also decomposition of the produced discharge products during the charge cycle.^[53] Carbon-based air electrodes have been used in a number of studies for Na-O₂ cells due to their unique carbonaceous properties such as excellent electrical conductivity, high surface area, light weight and controllable structure and porosity. Application of high surface area carbon materials with various porous structures and its correlation with discharge capacity and charge overpotential of the cell has been a major subject study within this field. Sun et al.^[6] demonstrated the use of diamond-like carbon (DLC) thin films air electrode as the first room-temperature Na-O₂ cell. DLC thin films in this study were deposited using r.f. sputtering using a carbon target. DLC thin film electrodes exhibited a specific discharge capacity of 1884 mAh g⁻¹ (0.56 mAh cm⁻²) at 1/10 C and 3600 mAh g⁻¹ (1.08 mAh cm⁻²) at 1/60 C in a carbonate-based electrolyte (Figure 13a).

Liu et al.^[15] reported the application of graphene nanosheets (GNS) air electrode in Na-O₂ cell. Thanks to the large surface area and excellent electrical conductivity of GNS, the electrode achieved a remarkable discharge capacity of 9268 mAh g⁻¹ at a current density of 200 mA g⁻¹. A nitrogen-doped graphene nanosheet (N-GNSs) analogue was also developed as an air electrode by our group and applied in Na-O₂ cells.^[16] N-GNSs air electrodes demonstrated a high discharge capacity of

8600 mAh g⁻¹ (3.6 mA cm⁻²) using a current density of 75 mA g⁻¹ (0.03 mA cm⁻²), a two fold increase in capacity compared to the pristine GNSs (Figure 14b). The significant high discharge capacity observed for N-GNSs air electrodes is attributed to its high surface area as well as presence of defective sites introduced by nitrogen doping in N-GNSs. On the other side, using a low surface area carbon fiber air electrode (<1 m² g⁻¹) in Na-O₂ cell by Hartmann et al.^[4,19] resulted in a low discharge capacity of 300 mAh g⁻¹ (2.9 mAh cm⁻²) at a current density of 12.3 mA g⁻¹ (0.1 mA cm⁻²) along with the formation of micrometer-sized discharge products (Figure 9a,b). Bender et al.^[40] also employed various carbon structures for Na-O₂ cells and reported similar discharge capacities as well as electrochemical characteristics. However, no correlation was concluded between the discharge capacity values and surface area of the air electrodes, since different active material loadings were used to make the air electrodes.

In order to systematically study the correlation between the discharge capacity of the Na-O₂ cell with the surface area and porosity of the air electrode, we developed a series of engineered carbon material with controllable porosity and surface area.^[26] By applying a heat-treatment procedure to the commercial carbon black we were able to precisely control the porosity and surface area of air electrode materials. The heat-treated electrode materials were then employed as an air electrode for Na-O₂ cells. Our studies determined that the discharge capacity of the air electrode can be linearly correlated with specific surface area of the electrode material within the mesopores range

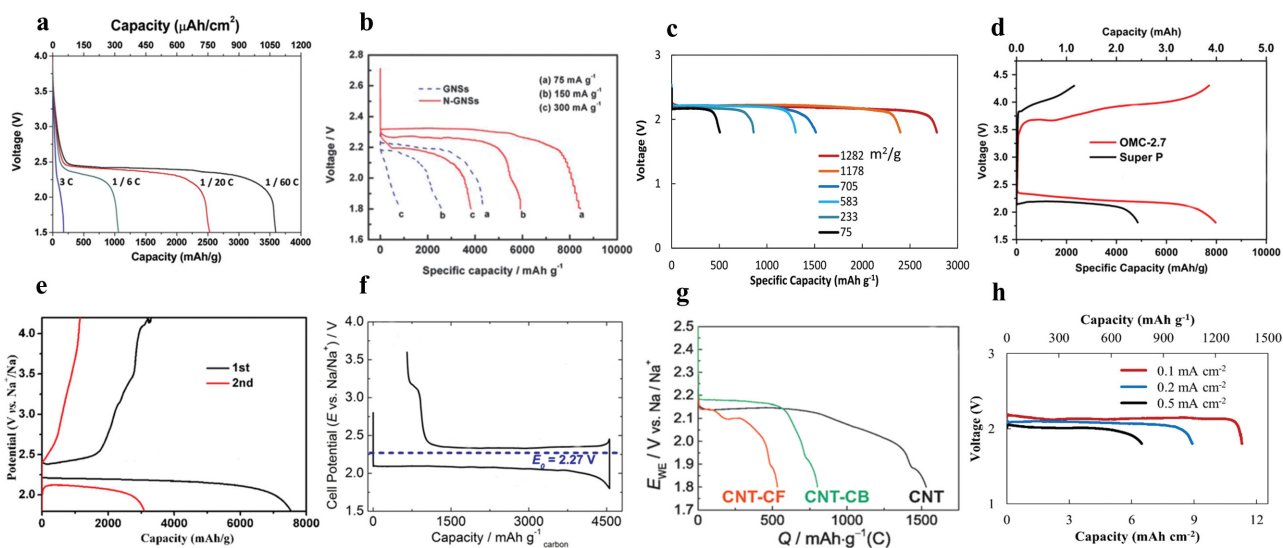


Figure 13. Application of carbonaceous air electrode with various architectures in Na-O₂ cells: a) diamond-like carbon (DLC) thin film discharged at 1/60C-3C in 1M NaPF₆/1:1 EC/DMC. a) Reproduced with permission.^[6] Copyright 2012, Elsevier. b) pristine and nitrogen-doped graphene nanosheets (GNS and N-GNS) discharged at 75–300 mA g⁻¹ in 0.5 M NaSO₃CF₃/DEGDME. b) Reproduced with permission.^[16] Copyright 2013, Royal Society of Chemistry. c) heat-treated carbon black with different specific surface area discharged at 75 mA g⁻¹ in 0.5 M NaSO₃CF₃/DEGDME. c) Reproduced with permission.^[26] Copyright 2014, Royal Society of Chemistry. d) ordered mesoporous carbon (OMC) discharged at 100 mA g⁻¹ in 0.5 M NaSO₃CF₃/PC. d) Reproduced with permission.^[25] Copyright 2015, Elsevier. e) carbon nanotube paper discharged at 500 mA g⁻¹ in 0.5 M NaTFSI/TEGDME. e) Reproduced with permission.^[18] Copyright 2014, Elsevier. f) vertically aligned carbon nanotubes (VACNTs) grown on stainless steel discharged at 67 mA g⁻¹ in 0.5 M NaSO₃CF₃/TEGDME. f) Reproduced with permission.^[22] Copyright 2014, Royal Society of Chemistry. g) carbon nanotubes (CNT), carbon nanotubes with added carbon nanofibers (CF-CNT) and carbon nanotubes with added carbon black (CB-CNT) discharged at 200 μA cm⁻² in 0.5 M NaOTf/DEGDME. g) Reproduced with permission.^[111] Copyright 2015, Wiley-VCH. h) nitrogen-doped carbon nanotubes on carbon paper (NCNT-CP) discharged at 0.1–0.5 mA cm⁻² in 0.5 M NaSO₃CF₃/DEGDME. h) Reproduced with permission.^[30] Copyright 2015, American Chemical Society.

(2–50 nm) (Figure 13c). More recently, Kwak et al.^[25] synthesized an ordered mesoporous carbon (OMC) material using hard template synthesis and evaluated it as an air electrode material for Na-O₂ cells. The OMC air electrode showed a specific discharge capacity of 7987 mAh g⁻¹ which was 1.6 times larger than that of carbon black in a carbonate solution, using a current density of 100 mA g⁻¹ (Figure 13d). However, sodium carbonate was detected as the major discharge product of cells, probably because of the decomposition of unstable carbonate solvent.

Carbon nanotubes (CNTs) are also widely used as the air electrode of the Na-O₂ cells. Jian et al.^[18] prepared a binder-free CNT paper as the air electrode of Na-O₂ cell with various electrolytes. The CNT paper exhibited the highest discharge capacity of 7530 mAh g⁻¹ at a current density of 500 mA g⁻¹ using 0.5 M NaSO₃CF₃/DEGDME electrolyte (Figure 13e). Zhao et al.^[22] also used vertically aligned carbon nanotubes (VACNTs) grown on stainless steel (SS) as the air electrode of Na-O₂ cell, where a discharge capacity of more than 4500 mAh g⁻¹ was obtained under a current density of 67 mA g⁻¹ (Figure 13f). In order to enhance the performance of the Na-O₂ cell, Bender et al.^[111] examined three different air electrode composed of pure CNT, CNT mixed with carbon fibers (CF), and CNT mixed with carbon black (CB). The pure CNT air electrode did not show a discharge capacity more than 1530 mAh g⁻¹ and adding 45% of CF and CB into CNT electrode decreased the electrode discharge capacity to 800 and 530 mAh g⁻¹, respectively (Figure 13g).

Our group also designed and fabricated a 3D structured air electrode based on vertically grown nitrogen doped CNT on carbon paper (NCNT-CP) as an air electrode for Na-O₂ cells.^[30] The binder-free NCNT-CP electrode was prepared using spray pyrolysis chemical vapor deposition (SPCVD) of NCNTs directly on the 3D structure of CP. The synthesized NCNT-CP air electrode exhibited dual macro/meso-porous structure, in which large micrometer sized pores could be found between the individual carbon fibers, allowing for an increase in transportation of oxygen and sodium ions while solid state discharge products can be captured within the mesopores space provided by the NCNTs. The NCNT-CP air electrode showed a remarkable discharge capacity of 11.3 mAh cm⁻² (17 times larger than CP) under a current density of 0.1 mA cm⁻². The elevated discharge capacity is a result of the increased surface area provided by NCNTs allowing for discharge product to form, while the micrometer sized pores of CP structure guarantee the continuous supply of oxygen and sodium ions onto the electrode surface. The discharge capacity of the Na-O₂ cells using NCNT-CP air electrode decreased by 1.7 times upon 5 times increase in the discharge current density (Figure 13h), indicating good rate capability of the air electrode. This enhanced rate capability is a result of sufficient supply of oxygen and sodium ions into the air electrode. Summarized in **Table 4** are the physical properties, experimental conditions and electrochemical responses of the carbonaceous air electrodes employed in Na-O₂ cells.

Table 4. A summary of physical properties, experimental conditions and electrochemical responses of the carbonaceous air electrodes employed in Na-O₂ cells.

Air electrode	BET Specific surface area	Specific Discharge Capacity	Discharge Current Density	Electrode Loading	Electrolyte	Ref.
Carbon fiber	< 1 m ² g ⁻¹	300 mAh g ⁻¹ (2.9 mAh cm ⁻²)	12.3 mA g ⁻¹ (0.12 mA cm ⁻²)	9.7 mg cm ⁻²	0.5 M NaSO ₃ CF ₃ / DEGDME	[4]
		12 mAh g ⁻¹ (0.11 mAh cm ⁻²)	51.4 mA g ⁻¹ (0.50 mA cm ⁻²)			
Diamond-like carbon (DLC)	-	3600 mAh g ⁻¹ (1.08 mAh cm ⁻²)	1/60 C	0.3 mg cm ⁻²	1 M NaPF ₆ EC/ DMC	[6]
		1884 mAh g ⁻¹ (0.56 mAh cm ⁻²)	1/10 C			
Heat-treated carbon black	1282 m ² g ⁻¹	2783 mAh g ⁻¹ (0.98 mAh cm ⁻²)	75 mA g ⁻¹ (0.03 mA cm ⁻²)	0.25 mg cm ⁻²	0.5 M NaSO ₃ CF ₃ / DEGDME	[26]
		1914 mAh g ⁻¹ (0.67 mAh cm ⁻²)	300 mA g ⁻¹ (0.10 mA cm ⁻²)			
ordered mesoporous carbon (OMC)	1544 m ² g ⁻¹	7987 mAh g ⁻¹ (1.57 mAh cm ⁻²)	100 mA g ⁻¹ (0.02 mA cm ⁻²)	~0.2 mg cm ⁻²	0.5 M NaSO ₃ CF ₃ /PC	[25]
Graphene nanosheets (GNSs)	83 m ² g ⁻¹	9268 mAh g ⁻¹	200 mA g ⁻¹	-	0.25 M NaPF ₆ /DME	[15]
Nitrogen-doped graphene nanosheets (N-GNSs)	-	1110 mAh g ⁻¹	1000 mA g ⁻¹	0.4 mg cm ⁻²	0.5 M NaSO ₃ CF ₃ / DEGDME	[16]
		8600 mAh g ⁻¹ (3.6 mAh cm ⁻²)	75 mA g ⁻¹ (0.03 mA cm ⁻²)			
Carbon nanotube (CNT) paper	-	3980 mAh g ⁻¹ (1.7 mAh cm ⁻²)	300 mA g ⁻¹ (0.12 mA cm ⁻²)	~0.2 mg cm ⁻²	0.5 M NaSO ₃ CF ₃ / DEGDME	[18]
		7530 mAh g ⁻¹ (=1.5 mAh cm ⁻²)	500 mA g ⁻¹ (0.1 mA cm ⁻²)			
vertically aligned carbon nanotubes (VACNTs)	80 m ² g ⁻¹	4500 mAh g ⁻¹ (=6.3 mAh cm ⁻²)	67 mA g ⁻¹ (0.09 mA cm ⁻²)	~1.5 mg cm ⁻²	0.5 M NaSO ₃ CF ₃ / TEGDME	[22]
CNT	215 m ² g ⁻¹	1530 mAh g ⁻¹ (4.22 mAh cm ⁻²)	65 mA g ⁻¹ (0.2 mA cm ⁻²)	0.6 g cm ⁻³	0.5 M NaSO ₃ CF ₃ / DEGDME	[111]
CNT-CF	112 m ² g ⁻¹	800 mAh g ⁻¹ (4.37 mAh cm ⁻²)	36 mA g ⁻¹ (0.2 mA cm ⁻²)	1.03 g cm ⁻³		
CNT-CB	128 m ² g ⁻¹	530 mAh g ⁻¹ (2.30 mAh cm ⁻²)	46 mA g ⁻¹ (0.2 mA cm ⁻²)	0.82 g cm ⁻³		
Nitrogen doped carbon nanotube-carbon paper (NCNT-CP)	27 m ² g ⁻¹	1349 mAh g ⁻¹ (11.3 mAh cm ⁻²)	12 mA g ⁻¹ (0.1 mA cm ⁻²)	0.24 mg cm ⁻²	0.5 M NaSO ₃ CF ₃ / DEGDME	[30]
		773 mAh g ⁻¹ (6.5 mAh cm ⁻²)	60 mA g ⁻¹ (0.5 mA cm ⁻²)			

5.2. Catalyst

Another effective route toward improving the electrochemical performance and reversibility of Li/Na-O₂ batteries is through the introduction of various catalysts into the air electrode. These catalytic centers are expected to promote the OER and ORR activities of the air electrode and accordingly overcome the sluggish kinetics in these batteries. The wisdom of exploring potential high performance electrocatalyst for alkali metal-O₂ batteries has been directionally guided by the tremendous precedential studies on OER/ORR catalyst for fuel cells. Consequently, noble metals and their alloys as well as non-noble metal oxides/nitrides/carbides have been widely applied for Li-O₂ batteries, which have been well-summarized in many other reviews.^[112–115] Although the electrocatalytic activity of these materials have been widely investigated, the mechanism

responsible for the catalytic activity is still a highly debated topic.^[53,65] On one side, initial formation of discharge products on the surface of the electrode during discharge is argued to rapidly reduce catalytic activity.^[65] For instance, McCloskey et al. demonstrated that conventional oxygen evolution electrocatalysis has no effects on Li-O₂ electrochemistry, but does influence the decomposition of electrolyte.^[116]

On the other side, there are a number of reports outlining the catalytic activity of noble and non-noble metals and metal oxides in Li-O₂ cells. It is believed that the ORR in non-aqueous metal-air cells is comprised of several consecutive electrochemical and non-electrochemical stages including: initial charge transfer to dissolve oxygen, appearance of a low soluble oxygen-metal intermediate, charge transfer stage into the prepared oxygen-metal intermediate and final agglomeration into globular metal oxide precipitate.^[53] Catalyst

may affect the specific reaction path taken and thus influence both appearance and structure of the oxygen-metal intermediates.^[53] Furthermore, use of catalysts may alter the size, structure, density and electronic conductivity of the metal-oxide products, since various intermediates present different mobility and diffusion rate.^[53] In such a way, it would be possible to explain the increase of the discharge capacity of metal-O₂ cells using an electrocatalyst as the air electrode. Formation of metal oxide products with increased conductivity in the presence of a catalyst may also result in an increase of discharge potential as well as a decrease in the charge overpotential for metal-O₂ cells.^[53] In a similar manner, design and application of suitable electrocatalysts for Na-O₂ cells may influence the discharge product composition and therefore cell overpotential.

Metal oxides, which have been the most common choices for Li-O₂ batteries, are also widely examined in Na-O₂ batteries. Rosenberg and Hintennach reported the application of α-MnO₂ nanowires for Na-air batteries, which presented a large initial capacity of 2056 mAh g⁻¹ but suffered 59% decrease in capacity after 2 cycles.^[117] Liu et al. reported a Ni foam@NiCo₂O₄ nanosheet electrode (Figure 14a), which exhibited a first discharge capacity of 1185 mAh g⁻¹ and maintained 401 mAh g⁻¹ after 10 cycles.^[83] Chen and co-workers developed a porous CaMnO₃ microspheres (Figure 14b), and tested it in Na-O₂ batteries.^[23] The CaMnO₃/C electrode

delivered a huge capacity of 9560 mAh g⁻¹ at a current density of 100 mA g⁻¹, which was nearly 2.5 times of that of bare carbon black electrode. The Na-O₂ cell with CaMnO₃/C electrode maintained 80 cycles with a restricted cut-off capacity of 1000 mAh g⁻¹. This prolonged cycle life is 8 times longer than bare carbon black (around 10 cycles). On the other hand, Zhang et al. combined Pt particles on graphene nanosheets (GNSs) to fabricate nanostructured Pt@GNSs catalyst for Na-O₂ batteries (Figure 14c).^[24] The discharge capacities of the cells increased from 5413 to 7574 mAh g⁻¹ after introducing Pt. The cell with Pt@GNSs catalyst was cycled for around 10 cycles with a cut-off capacity of 1000 mAh g⁻¹. The clogging of the pores and coverage of catalytic active sites due to aggregation of discharge products results in a decrease in catalytic performance during cell discharge. Therefore, the cycling performance of the cells is expected to improve with restricted cut-off capacities, which is consistent with aforementioned reports.

Besides the above-mentioned “solid-state” catalyst fixed at the substrates of air electrodes, a family of “soluble” catalysts is attracting more research interests. The concept of these catalysts are based on certain dissolved chemicals with suitable redox potentials into the electrolytes of Li/Na-O₂ batteries. These mobile catalytic centers can easily transport inside the cell and perform as redox mediators. The involved reactions can be demonstrated as follow:

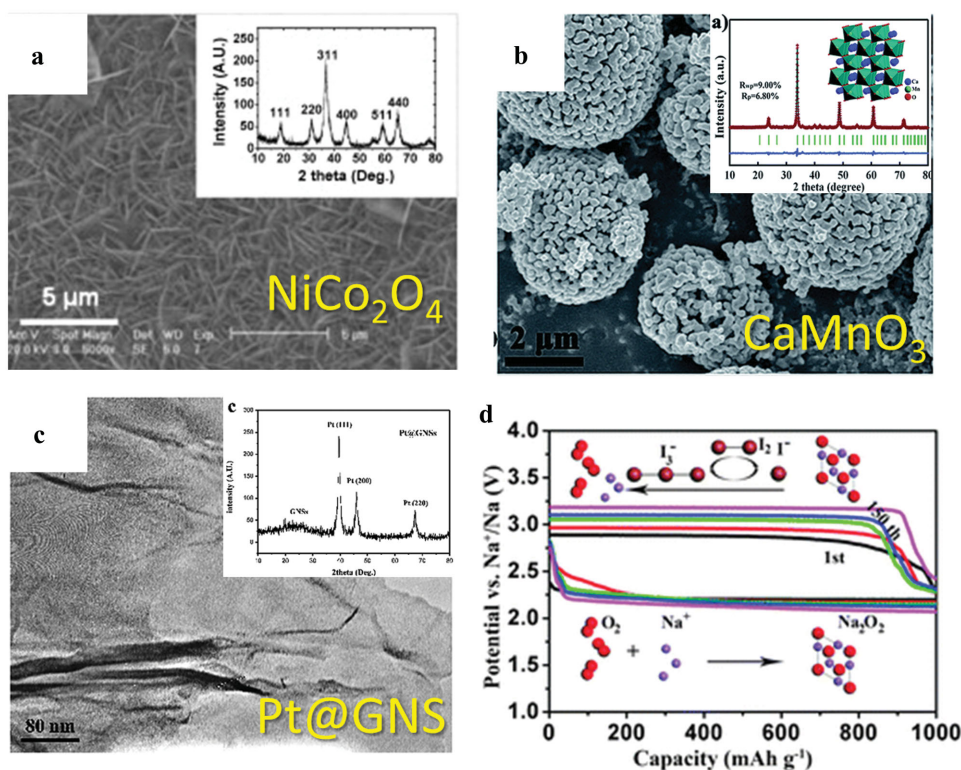
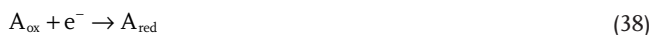
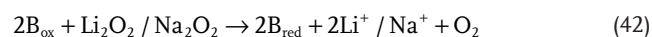


Figure 14. Typical catalysts adopted for Na-O₂ batteries. SEM and XRD patterns of (a) NiCo₂O₄, (b) CaMnO₃, and (c) Pt@graphene nanosheets air electrodes. d) Charge and discharge curves and schematic graph of a typical Na-O₂ cell with soluble NaI catalyst in electrolyte. a) Reproduced with permission.^[83] Copyright 2014, Elsevier. b) Reproduced with permission.^[23] Copyright 2015, Royal Society of Chemistry. c) Reproduced with permission.^[24] Copyright 2015, Royal Society of Chemistry. d) Reproduced with permission.^[126] Copyright 2015, Royal Society of Chemistry.

ORR:



OER:



Clearly, the required redox potential for ORR (discharge) and OER (charge) catalysts is different. Therefore, alternate mediators have been reported for enhancing ORR and OER reactions in Li/Na- O_2 batteries, respectively. Owen and co-workers demonstrated an ethyl viologen redox couple $\text{EtV}^{2+}/\text{EtV}^+$ as ORR catalyst with ionic liquid electrolyte in Li- O_2 cell.^[118] Afterward, four families of halide anions (e.g., Cl^- , Br^- , I^-), aromatic compounds, quinones/quinoids, and transition metal complexes were also reported to be active for oxygen evolution in metal-oxygen batteries.^[119] The effect of the soluble catalyst on OER reactions in Li- O_2 batteries has been shown to be remarkable. Bruce and co-workers found that tetrathiafulvalene (TTF) redox catalyst significantly reduced the charging potential of the Li- O_2 cell by around 0.6 V and enabled 100 consecutive discharge and charge cycles.^[120] Thereafter, various soluble catalysts were reported for Li- O_2 batteries.^[121–125]

Fu and co-workers reported the applicability of soluble NaI catalyst for Na- O_2 cell for the first time. The cell employing NaI soluble catalyst maintained 150 cycles with a cut-off discharge capacity of 1000 mAh g^{-1} (Figure 14d).^[126] Later, the same group also reported that the cycling life of Na- O_2 cell with soluble ferrocene catalyst can be further extended to 230 cycles using the same 1000 mAh g^{-1} cut-off capacity.^[127] These results highlight the efficiency of the redox mediator catalysts in Na- O_2 batteries. In addition, Nazar and co-workers proved that trace amount of H^+ (either from H_2O or other acid mediums) acts as a proton phase transfer catalyst (PPTC) and plays a critical role in determining: discharge capacity, NaO_2 morphology, and recharging behavior of Na- O_2 batteries.^[105] The authors synthesized pure home-made NaOTf salts via a chemical method to prepare a truly “water-free” electrolyte (0 ppm according to the authors). The Na- O_2 cell with “water-free” electrolyte exhibited diminished discharge capacity and elevated charge overpotential compared to the electrolyte containing commercial NaOTf. Interestingly, when a small amount of water (8 ± 1 ppm) or around 10 ppm of organic acid (benzoic and/or acetic acids) was intentionally added to this “water-free” electrolyte, the corresponding Na- O_2 cells exhibited similar electrochemical behavior to the cell with the electrolyte containing commercial NaOTf. To examine the charging (OER) process, the authors extracted NaO_2 air electrodes from a discharged cell with electrolyte containing 10 ppm water and tried to recharge them in either the same water-containing or water-free electrolyte. The authors observed a

low charging voltage plateau for the cell with water-containing electrolyte and a much higher voltage range, up to 4.5 V in the “water-free” electrolyte. Accordingly, the authors proposed that PPTC is critical for both ORR and OER processes of the Na- O_2 cell. Meanwhile, considering the reactivity between water/acid and metallic sodium anode, employing a protective membrane for a practical cell is also suggested by the authors. These results indicate that even in a “catalyst-free” design of Na- O_2 battery, trace amount of resident water in electrolyte contributes to reduce the charging overpotential of the cell, implying the indispensable role of catalysts in Na- O_2 batteries.

Overall, comparing to the numerous reports on the catalysts for Li-air batteries, the corresponding study on Na-air studies has been barely started. Nevertheless, rapid growth can be undoubtedly anticipated in this field in the near future. Various 3D structured solid-state catalysts or soluble catalysts can be expected for future Na- O_2 batteries.

6. Summary and Outlook

The Na- O_2 battery system has been developed as an alternative high energy density storage system with potential application in electric transportation. State of the art studies on Na- O_2 batteries brought a great deal of potential to achieve a high energy efficient battery system due to lower charging overpotential of Na- O_2 cells compared to Li- O_2 ones. However, there are also several challenges that should be addressed to further develop a long-life Na- O_2 rechargeable battery system.

Chemical composition of the discharge product in Na- O_2 cell is shown to be highly dependent on physicochemical conditions of the cell. Controlling the chemical composition of the Na- O_2 cell products is critically important, since the charging overpotential of the cell is dependent on the type of sodium oxides formed during the discharge cycle. Chemical composition of the Na- O_2 cell products can be manipulated by controlling the kinetic parameters of the cell. Reviewing the key studies on the Na- and Li- O_2 battery systems reveals that an oxygen-rich metal oxide phase may be produced by discharging the cells under a deficient oxygen condition. Higher discharge current density along with a high surface area air electrode and lower oxygen partial pressure is one route toward forming oxygen-rich metal oxide phases as the discharge products of Na- and Li- O_2 cells. In addition, finding a high-DN solvent with a relatively low HOMO level and a high pK_a is proven to be beneficial for Na- O_2 cells in terms of stabilizing the highly oxidative oxygen-rich discharge products produced in the cell. Further, recent studies on the cell chemistry revealed that Na- O_2 cells undergo less parasitic reactions compared to Li- O_2 . Nevertheless, formation and accumulation of parasitic side products as a result of decomposition of the electrolyte by highly oxidative discharge products in the cell still limits cycle life. Besides, sodium metal negative electrode and sodium oxide discharge product are more sensitive against trace amounts of moisture and carbon dioxide in the cell environment compared to the lithium counterparts which add more complexity to the cell design. Meanwhile, the critical role of proton in the reversibility of Na- O_2 batteries makes the precise control on the concentration of water or other proton donor in electrolyte even more challenging.

Morphology of the discharge products is another critical factor which can also be controlled by kinetics. Higher discharge current density and lower oxygen concentration in the electrochemical active sites may result in higher local overpotential during the discharge reaction. Higher local overpotential makes more nucleation sites energetically accessible and will result in amorphous as well as smaller particle size of the discharge products. More studies on the role of kinetics in alkali metal-O₂ cells are needed in order to truly understand the relation between the morphology of discharge products with kinetic parameters of the cell.

In-depth understanding of the chemistry and electrochemistry of Na-O₂ batteries will be further revealed with the use of various in situ technologies. These in situ characterizations can provide a more accurate insight into the real-time reactions that occur in Na-O₂ batteries. For example, Ganapathy et al. identified the difference between the decomposition routes of bulk Li₂O₂ and electrochemically discharged Li₂O₂ by in operando X-ray diffraction measurements.^[128] Also, Ortiz-Vitoriano et al. have shown that the discharge product NaO₂ in Na-O₂ batteries can rapidly transform after disassembling and exposing to ambient conditions even in an air-tight container.^[31] Therefore, various in situ technologies that have been adopted in Li-O₂ batteries (e.g., XRD,^[128–130] AFM,^[131] XPS,^[132] Raman,^[133] SEM,^[134] and XAS^[135]) should also be anticipated to play a more important role in Na-O₂ batteries as well.

Furthermore, the future design for a practical catalyst for Na-O₂ batteries should be subjected to the following guidance: (1) feasibility: the catalyst should be environmental benign, low cost, and preferred to be free of noble metal elements; (2) efficiency: the catalyst should significantly improve the capacities as well as maintain the low overpotential of the cell; and (3) advanced structure: catalyst with a 3D structure or loaded on a 3D structured skeleton is preferred, since it can provide abundant space to accommodate the discharge products. Advanced technologies such as atomic layer deposition (ALD)^[136,137] is anticipated to be adopted in the fabrication of these electrodes to meet the above-mentioned requirements.

At the time of writing this manuscript, the cycling performance of Na-O₂ cells is still generally poor, which can be attributed to a number of reasons. Apart from possible side reactions as a result of electrolyte and binder decomposition, impurities from injected gas, and oxidation of carbon-based electrodes, a major setback for Na-O₂ cells is related to the nature of the discharge products. On one side, the cell with Na₂O₂ as the discharge product suffers from high charging overpotential, similar to Li-O₂ cells. On the other side, the dissolving/precipitation mechanism of crystal growth in the case of NaO₂ results in the formation of micrometer-sized insulating cubes which may remain partially undecomposed following consecutive cycles.^[4] Besides, the growth of NaO₂ may also occur on insulating surfaces of the cell such as the separator, causing irreversible capacity loss.^[138] Future efforts on Na-O₂ cell should be conducted toward controlling the composition and morphology of the discharge product. The charging overpotential of the cell can be reduced by preventing electro/chemical conversion of NaO₂ to Na₂O₂ by employing appropriate electrolyte additives and (in)soluble catalysts. Meanwhile, precise control over the

nucleation and particle size of the NaO₂ product may also be achieved by manipulating the kinetic parameters of the cell.

Acknowledgements

H.Y. and Q.S. have contributed equally to this work. This study was supported by natural science and engineering research council of Canada, Canada research chair program, Canada foundation for innovation and the University of Western Ontario.

Received: September 6, 2015

Revised: December 10, 2015

Published online: June 3, 2016

- [1] J. B. Goodenough, K. S. Park, *J. Am. Chem. Soc.* **2013**, *135*, 1167.
- [2] P. G. Bruce, S. A. Freunberger, L. J. Hardwick, J. M. Tarascon, *Nat. Mater.* **2012**, *11*.
- [3] G. Girishkumar, B. McCloskey, A. C. Luntz, S. Swanson, W. Wilcke, *J. Phys. Chem. Lett.* **2010**, *1*, 2193.
- [4] P. Hartmann, C. L. Bender, M. Vracar, A. K. Durr, A. Garsuch, J. Janek, P. Adelhelm, *Nat. Mater.* **2013**, *12*, 228.
- [5] E. Peled, D. Golodnitsky, H. Mazon, M. Goor, S. Avshalomov, *J. Power Sources* **2011**, *196*, 6835.
- [6] Q. Sun, Y. Yang, Z. W. Fu, *Electrochem. Commun.* **2012**, *16*, 22.
- [7] Z. Q. Peng, S. A. Freunberger, L. J. Hardwick, Y. H. Chen, V. Giordani, F. Barde, P. Novak, D. Graham, J. M. Tarascon, P. G. Bruce, *Angew. Chem. Int. Ed.* **2011**, *50*, 6351.
- [8] S. A. Freunberger, Y. H. Chen, N. E. Drewett, L. J. Hardwick, F. Barde, P. G. Bruce, *Angew. Chem. Int. Ed.* **2011**, *50*, 8609.
- [9] M. M. O. Thotiyil, S. A. Freunberger, Z. Q. Peng, P. G. Bruce, *J. Am. Chem. Soc.* **2013**, *135*, 494.
- [10] F. Bardé, Y. Chen, L. Johnson, S. Schaltin, J. Fransaer, P. G. Bruce, *J. Phys. Chem. C* **2014**, *118*, 18892.
- [11] A. C. Luntz, B. D. McCloskey, *Chem. Rev.* **2014**, *114*, 11721.
- [12] B. D. McCloskey, A. Valery, A. C. Luntz, S. R. Gowda, G. M. Wallraff, J. M. Garcia, T. Mori, L. E. Krupp, *J. Phys. Chem. Lett.* **2013**, *4*, 2989.
- [13] B. D. McCloskey, A. Speidel, R. Scheffler, D. C. Miller, V. Viswanathan, J. S. Hummelshoj, J. K. Norkov, A. C. Luntz, *J. Phys. Chem. Lett.* **2012**, *3*, 997.
- [14] B. M. Gallant, R. R. Mitchell, D. G. Kwabi, J. Zhou, L. Zuin, C. V. Thompson, Y. Shao-Horn, *J. Phys. Chem. C* **2012**, *116*, 20800.
- [15] W. Liu, Q. Sun, Y. Yang, J. Y. Xie, Z. W. Fu, *Chem. Commun.* **2013**, *49*, 1951.
- [16] Y. Li, H. Yadegari, X. Li, M. N. Banis, R. Li, X. Sun, *Chem. Commun.* **2013**, *49*, 11731.
- [17] J. Kim, H. D. Lim, H. Gwon, K. Kang, *Phys. Chem. Chem. Phys.* **2013**, *15*, 3623.
- [18] Z. Jian, Y. Chen, F. Li, T. Zhang, C. Liu, H. Zhou, *J. Power Sources* **2014**, *251*, 466.
- [19] P. Hartmann, C. L. Bender, J. Sann, A. K. Durr, M. Jansen, J. Janek, P. Adelhelm, *Phys. Chem. Chem. Phys.* **2013**, *15*, 11661.
- [20] P. Hartmann, D. Gröbl, H. Sommer, J. Janek, W. G. Bessler, P. Adelhelm, *J. Phys. Chem. C* **2014**, *118*, 1461.
- [21] B. D. McCloskey, J. M. Garcia, A. C. Luntz, *J. Phys. Chem. Lett.* **2014**, *5*, 1230.
- [22] N. Zhao, C. Li, X. Guo, *Phys. Chem. Chem. Phys.* **2014**, *16*, 15646.
- [23] Y. Hu, X. Han, Q. Zhao, J. Du, F. Cheng, J. Chen, *J. Mater. Chem. A* **2015**, *3*, 3320.
- [24] S. Zhang, Z. Wen, K. Rui, C. Shen, Y. Lu, J. Yang, *J. Mater. Chem. A* **2015**, *3*, 2568.

- [25] W. J. Kwak, Z. Chen, C. S. Yoon, J. K. Lee, K. Amine, Y. K. Sun, *Nano Energy* **2015**, *12*, 123.
- [26] H. Yadegari, Y. Li, M. N. Banis, X. Li, B. Wang, Q. Sun, R. Li, T. K. Sham, X. Cui, X. Sun, *Energy Environ. Sci.* **2014**, *7*, 3747.
- [27] B. Lee, D. H. Seo, H. D. Lim, I. Park, K. Y. Park, J. Kim, K. Kang, *Chem. Mater.* **2014**, *26*, 1048.
- [28] S. Kang, Y. Mo, S. P. Ong, G. Ceder, *Nano Lett.* **2014**, *14*, 1016.
- [29] M. Balaish, A. Kraysberg, Y. Ein-Eli, *Phys. Chem. Chem. Phys.* **2014**, *16*, 2801.
- [30] H. Yadegari, M. N. Banis, B. Xiao, Q. Sun, X. Li, A. Lushington, B. Wang, R. Li, T. K. Sham, X. Cui, X. Sun, *Chem. Mater.* **2015**, *27*, 3040.
- [31] N. Ortiz-Vitoriano, T. P. Batcho, D. G. Kwabi, B. Han, N. Pour, K. P. C. Yao, C. V. Thompson, Y. Shao-Horn, *J. Phys. Chem. Lett.* **2015**, *6*, 2636.
- [32] C. O. Laoire, S. Mukerjee, K. M. Abraham, E. J. Plichta, M. A. Hendrickson, *J. Phys. Chem. C* **2009**, *113*, 20127.
- [33] A. Bard, L. Faulkner, *Electrochemical Methods: Fundamentals and Applications*, 2nd Ed., John Wiley & Sons, New York, **2001**.
- [34] X. D. Ren, Y. Y. Wu, *J. Am. Chem. Soc.* **2013**, *135*, 2923.
- [35] R. G. Pearson, *J. Am. Chem. Soc.* **1963**, *85*, 3533.
- [36] K. M. Abraham, *J. Electrochem. Soc.* **1996**, *143*, 1.
- [37] Z. Q. Peng, S. A. Freunberger, Y. H. Chen, P. G. Bruce, *Science* **2012**, *337*, 563.
- [38] M. M. Ottakam Thotiyil, S. A. Freunberger, Z. Peng, Y. Chen, Z. Liu, P. G. Bruce, *Nat. Mater.* **2013**, *12*, 1050.
- [39] P. Hartmann, C. L. Bender, J. Sann, A. K. Durr, M. Jansen, J. Janek, P. Adelhelm, *Phys. Chem. Chem. Phys.* **2013**, *15*, 11661.
- [40] C. L. Bender, P. Hartmann, M. Vra ar, P. Adelhelm, J. Janek, *Adv. Energy Mater.* **2014**, *4*, 1301863.
- [41] N. N. Greenwood, A. Earnshaw, *Chemistry of the Elements*, 2nd edn., Butterworth-Heinemann, Oxford, **1997**.
- [42] P. W. Gilles, J. L. Margrave, *J. Phys. Chem.* **1956**, *60*, 1333.
- [43] J. S. Kang, D. H. Kim, J. H. Hwang, J. Baik, H. J. Shin, M. Kim, Y. H. Jeong, B. I. Min, *Phys. Rev. B* **2010**, *82*, 193102.
- [44] J. J. Attema, G. A. de Wijs, R. A. de Groot, *J. Phys. Condens. Mat.* **2007**, *19*, 315212.
- [45] Y. N. Zhuravlev, N. G. Kravchenko, O. S. Obolonskaya, *Russ. J. Phys. Chem. B* **2010**, *4*, 20.
- [46] E. Bertel, N. Memmel, W. Jacob, V. Dose, F. P. Netzer, G. Rosina, G. Rangelov, G. Astl, N. Rosch, P. Knappe, B. I. Dunlap, H. Saalfeld, *Phys. Rev. B* **1989**, *39*, 6087.
- [47] N. G. Vannerberg, in *Progress in Inorganic Chemistry*, 4., John Wiley & Sons, New York, **1962**, pp. 125–197.
- [48] J. A. Creighton, E. R. Lippincott, *J. Chem. Phys.* **1964**, *40*, 1779.
- [49] J. Lu, L. Li, J. B. Park, Y. K. Sun, F. Wu, K. Amine, *Chem. Rev.* **2014**, *114*, 5611.
- [50] A. C. Luntz, B. D. McCloskey, *Chem. Rev.* **2014**, *114*, 11721.
- [51] J. Wang, Y. Li, X. Sun, *Nano Energy* **2013**, *2*, 443.
- [52] W. Xu, J. L. Wang, F. Ding, X. L. Chen, E. Nasybutin, Y. H. Zhang, J. G. Zhang, *Energy Environ. Sci.* **2014**, *7*, 513.
- [53] A. Kraysberg, Y. Ein-Eli, *Nano Energy* **2013**, *2*, 468.
- [54] C. L. Bender, B. Jache, P. Adelhelm, J. Janek, *J. Mater. Chem. A* **2015**, *3*, 20633.
- [55] B. D. McCloskey, D. S. Bethune, R. M. Shelby, G. Girishkumar, A. C. Luntz, *J. Phys. Chem. Lett.* **2011**, *2*, 1161.
- [56] S. A. Freunberger, Y. H. Chen, Z. Q. Peng, J. M. Griffin, L. J. Hardwick, F. Barde, P. Novak, P. G. Bruce, *J. Am. Chem. Soc.* **2011**, *133*, 8040.
- [57] K. Hayashi, K. Shima, F. Sugiyama, *J. Electrochem. Soc.* **2013**, *160*, A1467.
- [58] F. Liang, K. Hayashi, *J. Electrochem. Soc.* **2015**, *162*, A1215.
- [59] T. Hashimoto, K. Hayashi, *Electrochim. Acta* **2015**, *182*, 809.
- [60] S. H. Sahgong, S. T. Senthilkumar, K. Kim, S. M. Hwang, Y. Kim, *Electrochem. Commun.* **2015**, *51*, 53.
- [61] S. Yang, D. J. Siegel, *Chem. Mater.* **2015**, *27*, 3852.
- [62] R. B. Araujo, S. Chakraborty, R. Ahuja, *Phys. Chem. Chem. Phys.* **2015**, *17*, 8203.
- [63] M. D. Radin, D. J. Siegel, *Energy Environ. Sci.* **2013**, *6*, 2370.
- [64] O. Arcelus, C. Li, T. Rojo, J. Carrasco, *J. Phys. Chem. Lett.* **2015**, *6*, 2027.
- [65] J. Christensen, P. Albertus, R. S. Sanchez-Carrera, T. LOhmann, B. Kozinsky, R. Liedtke, J. Ahmed, A. Kojic, *J. Electrochem. Soc.* **2012**, *159*, R1.
- [66] Y. C. Lu, B. M. Gallant, D. G. Kwabi, J. R. Harding, R. R. Mitchell, M. S. Whittingham, Y. Shao-Horn, *Energy Environ. Sci.* **2013**, *6*, 750.
- [67] B. D. Adams, C. Radtke, R. Black, M. L. Trudeau, K. Zaghbi, L. F. Nazar, *Energy Environ. Sci.* **2013**, *6*, 1772.
- [68] D. Zhai, H. H. Wang, J. Yang, K. C. Lau, K. Li, K. Amine, L. A. Curtiss, *J. Am. Chem. Soc.* **2013**, *135*, 15364.
- [69] J. Yang, D. Zhai, H. H. Wang, K. C. Lau, J. A. Schlueter, P. Du, D. J. Myers, Y. K. Sun, L. A. Curtiss, K. Amine, *Phys. Chem. Chem. Phys.* **2013**, *15*, 3764.
- [70] H. G. Jung, J. Hassoun, J. B. Park, Y. K. Sun, B. Scrosati, *Nat. Chem.* **2012**, *4*, 579.
- [71] H. G. Jung, H. S. Kim, J. B. Park, I. H. Oh, J. Hassoun, C. S. Yoon, B. Scrosati, Y. K. Sun, *Nano Lett.* **2012**, *12*, 4333.
- [72] B. D. McCloskey, D. S. Bethune, R. M. Shelby, T. Mori, R. Scheffler, A. Speidel, M. Sherwood, A. C. Luntz, *J. Phys. Chem. Lett.* **2012**, *3*, 3043.
- [73] A. Khetan, H. Pitsch, V. Viswanathan, *J. Phys. Chem. Lett.* **2014**, *5*, 2419.
- [74] C. O. Laoire, S. Mukerjee, K. M. Abraham, E. J. Plichta, M. A. Hendrickson, *J. Phys. Chem. C* **2010**, *114*, 9178.
- [75] L. Johnson, C. Li, Z. Liu, Y. Chen, S. A. Freunberger, P. C. Ashok, B. B. Praveen, K. Dholakia, J. M. Tarascon, P. G. Bruce, *Nat. Chem.* **2014**, *6*, 1091.
- [76] S. Kang, Y. Mo, S. P. Ong, G. Ceder, *Chem. Mater.* **2013**, *25*, 3328.
- [77] M. D. Radin, J. F. Rodriguez, F. Tian, D. J. Siegel, *J. Am. Chem. Soc.* **2012**, *134*, 1093.
- [78] J. S. Hummelshoj, J. Blomqvist, S. Datta, T. Vegge, J. Rossmeisl, K. S. Thygesen, A. C. Luntz, K. W. Jacobsen, J. K. Nørskov, *J. Chem. Phys.* **2010**, *132*, 071101.
- [79] J. Z. Chen, J. S. Hummelshoj, K. S. Thygesen, J. S. G. Myrdal, J. K. Nørskov, T. Vegge, *Catal. Today* **2011**, *165*, 2.
- [80] V. Viswanathan, K. S. Thygesen, J. S. Hummelshoj, J. K. Nørskov, G. Girishkumar, B. D. McCloskey, A. C. Luntz, *J. Chem. Phys.* **2011**, *135*, 214704.
- [81] F. Tian, M. D. Radin, D. J. Siegel, *Chem. Mater.* **2014**, *26*, 2952.
- [82] Z. H. Cui, X. X. Guo, H. Li, *Energy Environ. Sci.* **2015**, *8*, 182.
- [83] W. M. Liu, W. W. Yin, F. Ding, L. Sang, Z. W. Fu, *Electrochem. Commun.* **2014**, *45*, 87.
- [84] Q. Sun, H. Yadegari, M. N. Banis, J. Liu, B. Xiao, B. Wang, S. Lawes, X. Li, R. Li, X. Sun, *Nano Energy* **2015**, *12*, 698.
- [85] R. R. Mitchell, B. M. Gallant, Y. Shao-Horn, C. V. Thompson, *J. Phys. Chem. Lett.* **2013**, *4*, 1060.
- [86] S. R. Gowda, A. Brunet, G. M. Wallraff, B. D. McCloskey, *J. Phys. Chem. Lett.* **2013**, *4*, 276.
- [87] H. K. Lim, H. D. Lim, K. Y. Park, D. H. Seo, H. Gwon, J. Hong, W. A. Goddard, H. Kim, K. Kang, *J. Am. Chem. Soc.* **2013**, *135*, 9733.
- [88] Y. S. Mekonnen, K. B. Knudsen, J. S. G. Myrdal, R. Younesi, J. Hojberg, J. Hjelm, P. Norby, T. Vegge, *J. Chem. Phys.* **2014**, *140*, 121101.
- [89] J. S. Hummelshoj, A. C. Luntz, J. K. Nørskov, *J. Chem. Phys.* **2013**, *138*, 034703.
- [90] Y. C. Lu, E. J. Crumlin, T. J. Carney, L. Baggetto, G. M. Veith, N. J. Dudney, Z. Liu, Y. Shao-Horn, *J. Phys. Chem. C* **2013**, *117*, 25948.
- [91] T. Zhang, H. S. Zhou, *Nat. Commun.* **2013**, *4*, 1817.
- [92] K. Takechi, T. Shiga, T. Asaoka, *Chem. Commun.* **2011**, *47*, 3463.

- [93] Y. Liu, R. Wang, Y. Lyu, H. Li, L. Chen, *Energy Environ. Sci.* **2014**, 7, 677.
- [94] S. K. Das, S. Xu, L. A. Archer, *Electrochem. Commun.* **2013**, 27, 59.
- [95] S. M. Xu, Y. Y. Lu, H. S. Wang, H. D. Abruna, L. A. Archer, *J. Mater. Chem. A* **2014**, 2, 17723.
- [96] S. Meini, M. Piana, N. Tsiouvaras, A. Garsuch, H. A. Gasteiger, *Electrochem. Solid St.* **2012**, 15, A45.
- [97] Z. Y. Guo, X. L. Dong, S. Y. Yuan, Y. G. Wang, Y. Y. Xia, *J. Power Sources* **2014**, 264, 1.
- [98] M. H. Cho, J. Trottier, C. Gagnon, P. Hovington, D. Clement, A. Vijh, C. S. Kim, A. Guerfi, R. Black, L. Nazar, K. Zaghib, *J. Power Sources* **2014**, 268, 565.
- [99] N. B. Aetukuri, B. D. McCloskey, J. M. Garcia, L. E. Krupp, V. Viswanathan, A. C. Luntz, *Nat. Chem.* **2015**, 7, 50.
- [100] K. U. Schwenke, M. Metzger, T. Restle, M. Piana, H. A. Gasteiger, *J. Electrochem. Soc.* **2015**, 162, A573.
- [101] S. Meini, S. Solchenbach, M. Piana, H. A. Gasteiger, *J. Electrochem. Soc.* **2014**, 161, A1306.
- [102] F. Li, S. Wu, D. Li, T. Zhang, P. He, A. Yamada, H. Zhou, *Nat. Commun.* **2015**, doi:10.1038/ncomms8843.
- [103] T. Liu, M. Leskes, W. Yu, A. J. Moore, L. Zhou, P. M. Bayley, G. Kim, C. P. Grey, *Science* **2015**, 350, 530.
- [104] Q. Sun, H. Yadegari, M. N. Banis, J. Liu, B. Xiao, X. Li, C. Langford, R. Li, X. Sun, *J. Phys. Chem. C* **2015**, 119, 13433.
- [105] C. Xia, R. Black, R. Fernandes, B. Adams, L. F. Nazar, *Nat. Chem.* **2015**, 7, 496.
- [106] R. Black, S. H. Oh, J. H. Lee, T. Yim, B. Adams, L. F. Nazar, *J. Am. Chem. Soc.* **2012**, 134, 2902.
- [107] E. Nasybulin, W. Xu, M. H. Engelhard, Z. M. Nie, X. H. S. Li, J. G. Zhang, *J. Power Sources* **2013**, 243, 899.
- [108] C. V. Amanchukwu, J. R. Harding, Y. Shao-Horn, P. T. Hammond, *Chem. Mater.* **2015**, 27, 550.
- [109] J. Heine, U. Rodehorst, J. P. Badillo, M. Winter, P. Bieker, *Electrochim. Acta* **2015**, 155, 110.
- [110] J. R. Harding, C. V. Amanchukwu, P. T. Hammond, Y. Shao-Horn, *J. Phys. Chem. C* **2015**, 119, 6947.
- [111] C. L. Bender, W. Bartuli, M. G. Schwab, P. Adelhelm, J. Janek, *Energy Technology* **2015**, 3, 242.
- [112] R. Black, J. H. Lee, B. Adams, C. A. Mims, L. F. Nazar, *Angew. Chem. Int. Ed.* **2013**, 52, 392.
- [113] F. J. Li, T. Zhang, H. S. Zhou, *Energy Environ. Sci.* **2013**, 6, 1125.
- [114] Z. L. Wang, D. Xu, J. J. Xu, X. B. Zhang, *Chem. Soc. Rev.* **2014**, 43, 7746.
- [115] M. D. Bhatt, H. Geaney, M. Nolan, C. O'Dwyer, *Phys. Chem. Chem. Phys.* **2014**, 16, 12093.
- [116] B. D. McCloskey, R. Scheffler, A. Speidel, D. S. Bethune, R. M. Shelby, A. C. Luntz, *J. Am. Chem. Soc.* **2011**, 133, 18038.
- [117] S. Rosenberg, A. Hintennach, *J. Power Sources* **2015**, 274, 1043.
- [118] M. J. Lacey, J. T. Frith, J. R. Owen, *Electrochem. Commun.* **2013**, 26, 74.
- [119] G. V. Chase, S. Zecevic, T. W. Wesley, J. Uddin, K. A. Sasaki, P. G. Vincent, V. Bryantsev, M. Blanco, D. D. Addison, US Pat. 0028137 A1, 2012.
- [120] Y. Chen, S. A. Freunberger, Z. Peng, O. Fontaine, P. G. Bruce, *Nat. Chem.* **2013**, 5, 489.
- [121] B. J. Bergner, A. Schurmann, K. Pepler, A. Garsuch, J. Janek, *J. Am. Chem. Soc.* **2014**, 136, 15054.
- [122] D. Sun, Y. Shen, W. Zhang, L. Yu, Z. Yi, W. Yin, D. Wang, Y. Huang, J. Wang, D. Wang, J. B. Goodenough, *J. Am. Chem. Soc.* **2014**, 136, 8941.
- [123] H. D. Lim, H. Song, J. Kim, H. Gwon, Y. Bae, K. Y. Park, J. Hong, H. Kim, T. Kim, Y. H. Kim, X. Lepro, R. Ovalle-Robles, R. H. Baughman, K. Kang, *Angew. Chem. Int. Ed.* **2014**, 53, 3926.
- [124] C. Li, O. Fontaine, S. A. Freunberger, L. Johnson, S. Grugeon, S. Laruelle, P. G. Bruce, M. Armand, *J. Phys. Chem. C* **2014**, 118, 3393.
- [125] S. Matsuda, S. Mori, Y. Kubo, K. Uosaki, K. Hashimoto, S. Nakanishi, *Chem. Phys. Lett.* **2015**, 620, 78.
- [126] W. W. Yin, Z. Shadike, Y. Yang, F. Ding, L. Sang, H. Li, Z. W. Fu, *Chem. Commun.* **2015**, 51, 2324.
- [127] W. W. Yin, J. L. Yue, M. H. Cao, W. Liu, J. J. Ding, F. Ding, L. Sang, Z. W. Fu, *J. Mater. Chem. A* **2015**, 3, 19027.
- [128] S. Ganapathy, B. D. Adams, G. Stenou, M. S. Anastasaki, K. Goubitz, X. F. Miao, L. F. Nazar, M. Wagemaker, *J. Am. Chem. Soc.* **2014**, 136, 16335.
- [129] H. Lim, E. Yilmaz, H. R. Byon, *J. Phys. Chem. Lett.* **2012**, 3, 3210.
- [130] M. M. Storm, R. E. Johnsen, R. Younesi, P. Norby, *J. Mater. Chem. A* **2015**, 3, 3113.
- [131] R. Wen, M. Hong, H. R. Byon, *J. Am. Chem. Soc.* **2013**, 135, 10870.
- [132] Y. C. Lu, E. J. Crumlin, G. M. Veith, J. R. Harding, E. Mutoro, L. Baggetto, N. J. Dudney, Z. Liu, Y. Shao-Horn, *Sci. Rep.* **2012**, 2, 715.
- [133] F. S. Gittleston, W. H. Ryu, A. D. Taylor, *ACS Appl. Mater. Interfaces* **2014**, 6, 19017.
- [134] H. Zheng, D. Xiao, X. Li, Y. Liu, Y. Wu, J. Wang, K. Jiang, C. Chen, L. Gu, X. Wei, Y. S. Hu, Q. Chen, H. Li, *Nano Lett.* **2014**, 14, 4245.
- [135] G. S. Hutchings, J. Rosen, D. Smiley, G. R. Goward, P. G. Bruce, F. Jiao, *J. Phys. Chem. C* **2014**, 118, 12617.
- [136] X. Meng, X. Q. Yang, X. Sun, *Adv. Mater.* **2012**, 24, 3589.
- [137] J. Liu, X. Sun, *Nanotechnology* **2015**, 26, 024001.
- [138] P. Hartmann, M. Heinemann, C. L. Bender, K. Graf, R. P. Baumann, P. Adelhelm, C. Heiliger, J. Janek, *J. Phys. Chem. C* **2015**, 119, 22778.